Ocean Modelling 87 (2015) 30–47

Contents lists available at ScienceDirect

Ocean Modelling

journal homepage: www.elsevier.com/locate/ocemod

Scaling depth-induced wave-breaking in two-dimensional spectral wave models

J.E. Salmon *, L.H. Holthuijsen, M. Zijlema, G.Ph. van Vledder, J.D. Pietrzak

Faculty of Civil Engineering and Geosciences, Delft University of Technology, Stevinweg 1, 2628CN Delft, The Netherlands

ARTICLE INFO

Article history:
Received 6 May 2014
Received in revised form 17 December 2014
Accepted 27 December 2014
Available online 13 January 2015

Keywords:
Coastal zone
Wave breaking
Surf zone
Wave dissipation
Wave model
Coastal systems

ABSTRACT

Wave breaking in shallow water is still poorly understood and needs to be better parameterized in 2D spectral wave models. Significant wave heights over horizontal bathymetries are typically under-predicted in locally generated wave conditions and over-predicted in non-locally generated conditions. A joint scaling dependent on both local bottom slope and normalized wave number is presented and is shown to resolve these issues. Compared to the 12 wave breaking parameterizations considered in this study, this joint scaling demonstrates significant improvements, up to ~50% error reduction, over 1D horizontal bathymetries for both locally and non-locally generated waves. In order to account for the inherent differences between uni-directional (1D) and directionally spread (2D) wave conditions, an extension of the wave breaking dissipation models is presented. By including the effects of wave directionality, rms-errors for the significant wave height are reduced for the best performing parameterizations in conditions with strong directional spreading. With this extension, our joint scaling improves modeling skill for significant wave heights over a verification data set of 11 different 1D laboratory bathymetries, 3 shallow lakes and 4 coastal sites. The corresponding averaged normalized rms-error for significant wave height in the 2D cases varied between 8% and 27%. In comparison, using the default setting with a constant scaling, as used in most presently operating 2D spectral wave models, gave equivalent errors between 15% and 38%.

1. Introduction

Predicting breaking waves in shallow water under complex 2D bathymetry and current conditions is important for understanding the natural development of oceanic islands and coastal regions, the design and management of man-made coastal structures, and risk assessment. Such waves usually dissipate in a relatively narrow 1D surf zone fringing the coast. However, occasionally a surf zone may occur suddenly and with catastrophic effect over a large 2D region when low-lying land, an island or a reef is inundated in a severe storm. Waves have been shown to be vitally important in understanding processes such as sediment re-suspension and transport in estuaries (e.g. Green and Coco, 2014) and the exchanges between the nearshore and inner shelf (Lentz et al., 2008). Furthermore, the increase in the need for interdisciplinary research to understand these complex processes has led to an increased use of coupling phase-averaging wave models to flow and circulation models (e.g. Dietrich et al., 2013).

Phase-averaged spectral wave models are widely used to describe the sea-state with waves described with a 2D energy spectrum, defined at each location and moment in time as the distribution of wave energy over frequency and direction of the constituent wave components (Phillips, 1977; WAMDI, 1988; Holthuijsen, 2007). Within the limitations of stationary Gaussian processes, a variety of statistical wave parameters can be estimated from the spectrum such as the significant wave height, defined as the mean wave height of the one-third highest waves (Longuet-Higgins, 1952). The most advanced of these models are the so-called third-generation wave models where the non-linear quadruplet wave–wave interactions are explicitly represented, permitting a development of the wave spectrum that is unrestrained by a priori assumptions. This is in contrast to first- and second-generation wave models where quadruplet interactions are not represented or are represented by simple parameterizations (Komen et al., 1994). This difference allows third-generation wave models to freely develop the spectrum in arbitrary 2D conditions of wind, currents and bathymetry as the spectral shape is not enforced a priori (Holthuijsen, 2007). We conform to this

* Corresponding author.
E-mail addresses: salmonjames@gmail.com (J.E. Salmon), l.h.holthuijsen@tudelft.nl (L.H. Holthuijsen), m.zijlema@tudelft.nl (M. Zijlema), g.p.vanvledder@tudelft.nl (G.Ph. van Vledder), j.d.pietrzak@tudelft.nl (J.D. Pietrzak).

http://dx.doi.org/10.1016/j.ocemod.2014.12.011
1463-5003/

commonly accepted practice despite the fact that such models still typically use parametric expressions for the remaining wave processes e.g. white capping and wind input. Operational models of this type are WAM (WAMDI group, 1988; Komen et al., 1994; Monbaliu et al., 2000), WAVEWATCH III (Tolman, 1990a, 2009; Tolman and Chalikov, 1996), TOMAWAC (Benoit et al., 1996), SWAN (Booij et al., 1999; Ris et al., 1999; Zijlema, 2010), MIKE21SW (Sørensen et al., 2004), CREST (Ardhuin et al., 2001) and WWM (Roland et al., 2006; Roland, 2009).

The default parameterization for depth-induced wave breaking dissipation, used in most of these models, is one based on an analogy of the dissipation in a 1D bore (Lamb, 1932; Stoker, 1957; LeMéhauté, 1962) introduced by Battjes and Janssen (1978). It combines the dissipation of a single breaking wave with a Rayleigh distribution for random wave heights. From this, three dissipation models were developed: Battjes and Janssen (1978), Thornton and Guza (1983) and Baldock et al. (1998). They are subsequently referred to as the BJ78, TG83 and B98 models. The essential difference is how they represent the statistics of the breaking waves (see Fig. 1; top panel).

Battjes and Janssen (1978) truncate the distribution of the wave heights at an upper limit given by the maximum possible wave height for a given depth $H = H_{max}$ where they assume a delta function in the distribution (with a surface area equal to the probability of exceeding $H = H_{max}$ if the complete Rayleigh distribution would apply). As shown in Fig. 1(A), this delta function represents the assumption that all breaking waves have the same wave height H_{max}. A reduced breaking criterion of Miche (1944) is then used to scale the dissipation with a fixed ratio of the maximum possible wave height H_{max} and the local depth d, denoted as $\gamma_{BJ} = H_{max}/d$. Battjes and Janssen (1978) used $\gamma_{BJ} = 0.8$ in their computations, but most third-generation models use $\gamma_{BJ} = 0.73$, a value averaged from the more extensive data set of Battjes and Stive (1985, their Table 1). For convenience, we subsequently refer to this parameterization for dissipation and γ-scaling as the BJ model.

Thornton and Guza (1983, Fig. 1B) suggest, on the basis of their field observations, using a Rayleigh distribution for the breaking waves shifted to higher wave heights instead. This is achieved through the use of a weighting function with a scaling coefficient $M_{TG} = (H_{rms}/\gamma_{TG}d)^n$ where $n = 2$ and $\gamma_{TG} = H_{rms,max}/d$ is the ratio of the maximum possible root-mean-square wave height to depth.

Baldock et al. (1998, Fig. 1C) also suggest using a Rayleigh distribution but truncated at a lower limit of $H_b = \gamma_B d$ (the minimum breaker height) to represent the breaking wave height distribution. Their expression for dissipation is subsequently corrected by Janssen (2006), Janssen and Battjes (2007) and Alsina and Baldock (2007). An overview of variable parameterizations for

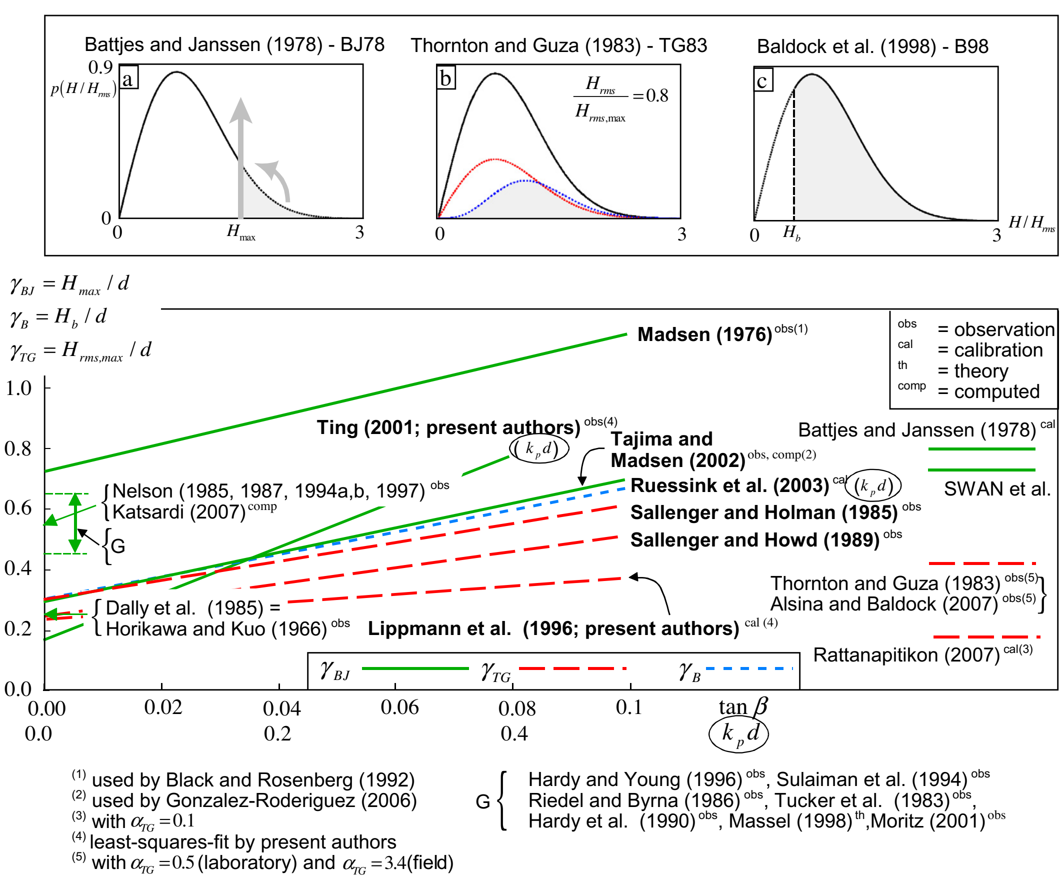

Fig. 1. The parameterization of depth-induced wave breaking. The top panels illustrate the representation of the breaking waves with the Rayleigh probability density function (in black) for the (a) Battjes and Janssen (1978; BJ), (b) Thornton and Guza (1983; TG) and (c) Baldock et al. (1998; B) dissipation models. The delta function used in BJ78 is represented by a vertical arrow in (a). Both expressions of Thornton and Guza (1983, their Eqs. (20) and (21)) are shown in (b) as the red and blue lines respectively for $H_{rms}/\gamma_{TG}d = 0.8$. The lower panel presents the ratio of critical wave height over depth, which is used to scale the dissipation models, as a function of bottom slope $\tan\beta$ or normalized wave number k_pd. The seven varying scalings considered in this study are labeled in bold type. All expressions are based on direct observations of individual waves except when indicated otherwise (see inset). All expressions have been derived for irregular waves (or have been used for irregular waves as indicated). The values of γ at $\tan\beta = 0$ from reference group G cluster between 0.45 and 0.65. Constant values are indicated at the right-hand side of the diagram with horizontal lines. The commonly used value $\gamma_{BJ} = 0.73$ in third-generation models (indicated with SWAN et al.) has been added as reference. (For interpretation of the references to color in this figure legend, the reader is referred to the web version of this article.)

γ_{BJ}, γ_{TG} and γ_B is given in Fig. 1 (bottom panel) and a more extensive overview is presented in Appendix A.

However, several studies have shown that when waves are locally generated over a (near-) horizontal bathymetry, the BJ model over-estimates the dissipation (de Waal, 2002; Bottema and Beyer, 2002; Bottema et al., 2002; van der Westhuysen et al., 2007; Bottema and van Vledder, 2009; Groeneweg et al., 2008; van Vledder et al., 2008; Goda, 2009). van der Westhuysen (2009, 2010) addresses this problem by scaling TG83 using bi-phase characteristics of the waves and shows that in a storm over the Wadden Sea, the under-prediction of the significant wave height is reduced. However, if waves are *not* locally generated but arrive from a distant source, we find that this formulation over-estimates the significant wave height e.g. during storm observations in a $10 \times 10\,\mathrm{km}^2$ shallow coastal bay (Haringvliet; see Section 5.2).

In this paper, we present a new parameterization for depth-induced wave breaking for 2D spectral wave models which addresses this dichotomy by considering both the effects of local bottom slope and normalized wave number in a joint γ-scaling. Furthermore, we demonstrate the limitations of the assumption of a 1D bore in the parameterization when used for strongly 2D conditions and present an extension for these models to account for the enhanced wave directionality under such conditions.

This paper is structured as follows. First, in Section 2, we describe the wave model used in this study and in Section 3, we describe our methodology. In Section 4, we present our new scaling for γ which depends both on local bottom slope and normalized wave number. We also present an extension to include wave directionality. In Section 5, we demonstrate the shortcomings of currently available parameterizations used in all third-generation wave models through a comparison of computed significant wave heights with both laboratory and field observations. An analysis of the error characteristics highlights the need for a joint dependency on both local bottom slope and normalized wave number for γ which we investigate with our new parameterization in Section 6. Here, we show large improvements for significant wave heights for locally and non-locally generated waves over 1D horizontal bathymetries. Finally, in Section 7, we conclude with a discussion of our results with a particular focus on the 2D field cases and the extension to include wave directionality.

2. Model description

The wave model used in this study is the third-generation wave model SWAN version 40.91 (Simulating WAves Nearshore; Booij et al., 1999). However, any of the third-generation wave models outlined in the Introduction are equally applicable. It solves the wave action density, defined as the ratio of energy over the relative frequency (Bretherton and Garrett, 1968; Phillips, 1977, p. 26) with a spectral balance in Cartesian x, y coordinates:

$$\frac{\partial N(\sigma,\theta;x,y,t)}{\partial t}+\frac{\partial c_{g,x}N(\sigma,\theta;x,y,t)}{\partial x}+\frac{\partial c_{g,y}N(\sigma,\theta;x,y,t)}{\partial y}+\frac{\partial c_{\theta}N(\sigma,\theta;x,y,t)}{\partial \theta}+\frac{\partial c_{\sigma}N(\sigma,\theta;x,y,t)}{\partial \sigma}=\frac{S(\sigma,\theta;x,y,t)}{\sigma} \quad (1)$$

where $N(\sigma,\theta) = E(\sigma,\theta)/\sigma$ represents the action density with the energy density $E(\sigma,\theta)$ as a function of the relative radian frequency σ and spectral direction θ. The left-hand side terms of Eq. (1) represent, respectively, the rate of change of $N(\sigma,\theta)$ in time and the propagation of $N(\sigma,\theta)$ in geographical space, θ-space and σ-space with propagation velocities $c_{g,x}$, $c_{g,y}$, c_θ, c_σ. The right-hand side represents the source terms for action density including wave generation by wind, nonlinear wave–wave interactions (triad and quadruplet interactions) and dissipation terms for white capping, bottom friction and depth-induced breaking.

All computations with SWAN were carried out in stationary mode. For laboratory cases, we use only the source terms for triad wave–wave interactions (the Lumped Triad Approximation (LTA) of Eldeberky (1996)), bottom friction (Hasselmann et al., 1973) with bottom friction coefficient $0.038\,\mathrm{m}^2\,\mathrm{s}^{-3}$ (Zijlema et al., 2012) and depth-induced breaking. Additionally, for field cases, we include the generation by wind of Snyder et al. (1981) as adapted by Komen et al. (1984) with wind drag coefficient calculated as described by Zijlema et al. (2012), quadruplet wave–wave interactions with the Discrete Interaction Approximation (DIA) of Hasselmann et al. (1985) scaled for shallow water as suggested by the WAMDI group (1988) and white capping with the pulse model of Hasselmann (1974) as modified by the WAMDI group (1988) and shifted to higher frequencies as suggested by Rogers et al. (2003). All these settings are the current default physics in SWAN from version 40.91A apart from the bottom friction and wind drag coefficient, and the depth-induced breaking source term which is the focus of this paper.

The only exception to the above was for our reef field case (Guam) where we used a spectral version of the bottom friction model of Thornton and Guza (1983) as bottom friction estimates were available for this friction model (Péquignet et al., 2011; see Supplementary Materials). We distribute the corresponding bulk dissipation for bottom friction proportionally to the spectral density of the near-bottom velocity from linear theory (Graber and Madsen, 1988; Tolman, 1990b) given by:

$$S_{bf}(\sigma,\theta) = A\left(\frac{\sigma}{\sinh(kd)}\right)^2 E(\sigma,\theta) \quad (2)$$

where A is such that the bulk dissipation is given by the Thornton and Guza (1983) model calculated with characteristic frequency f_{m01} (defined below).

All laboratory cases and, in view of their idealized character, all lake cases were computed in 1D. For the field cases, the computations were 2D using either regular grids (Haringvliet and Petten) or curvi-linear grids (Amelander Zeegat and Guam). For all laboratory cases, a logarithmic frequency distribution with frequency resolution $\Delta f = 0.05f$ and directional resolution of $\Delta\theta = 0.5^0$ was used. For all lake and field cases, $\Delta f = 0.1f$ (a constraint of the DIA) and $\Delta\theta = 15^0$. The default criteria for stopping SWAN computations was applied i.e., a change of less than 2% in the significant wave height and mean wave period over 98% of the spatial computational grid points between one iteration and the next; capped at 50 iterations. This cap was verified to be sufficient for the default stopping criteria.

All integral wave parameters such as the significant wave height and mean wave frequencies are estimated in the present study from the moments of the 1D variance density spectrum $m_n = \int \sigma^n E'(\sigma)\,d\sigma$ where $E'(\sigma) = \int E(\sigma,\theta)\,d\theta/(\rho g)$ with ρ, the density of water and g, the gravitational acceleration. The significant wave height is computed as $H_{m0} = 4\sqrt{m_0}$ and the mean frequency as $f_{m01} = m_1/m_0$.

3. Methodology

This section begins with our selection of parameterizations for wave breaking applicable for use in 2D spectral models over an extensive range of irregular (i.e., random) waves over 1D and 2D bathymetries. We subsequently present the observations used, including the selection of calibration and validation subsets, and our method of analysis.

3.1. Depth-induced wave breaking models

In this section, we select γ-scalings for depth-induced wave breaking suitable for irregular waves over 1D and 2D bathymetries. We include in our verification all three versions of the basic Battjes and Janssen (1978) dissipation model described in the Introduction. However, we discount γ-scalings that are limited to 1D situations and are parameterized in terms of *incident* wave parameters as such scalings cannot be used in 2D wave models. Such parameters include offshore wave steepness (Battjes and Stive, 1985; Svendsen, 1987; Nairn, 1990; Rattanapitikon et al., 2003a; Holthuijsen and Booij, 2006; Camenen and Larson, 2007), offshore wave height (Apotsos et al., 2008) and deep water wave length (Goda, 2004). For 2D situations, these parameters vary along the coast and lose much of their relevance for the surf zone when other processes apart from breaking, for instance refraction, affect the waves. In addition, van der Westhuysen (2010, his Fig. 9) demonstrates that offshore, or even local, wave steepness (Vink, 2001) is unable to represent γ_{BJ} satisfactory. Finally, we do not consider studies which obtain results for regular waves which do not seem to apply to irregular waves (Vincent, 1985; Kamphuis, 1991; Goda, 2010).

Based on the above arguments and the review of van der Westhuysen (2010), we select seven γ-scalings which vary with local parameters; namely local bottom slope or characteristic normalized wave number. These are presented in Fig. 1 (bottom panel). For Ruessink et al. (2003), we use both the original and corrected B98 model. We also include the recent versions of van der Westhuysen (2009) and Filipot and Ardhuin (2012) of the TG83 model as they offer alternatives to using a variable γ value. The BJ model, with a constant $\gamma_{BJ} = 0.73$, is included only as a reference.

The only conceptual alternative to the Battjes and Janssen (1978) approach, that we are aware of, is given by Dally et al. (1985) who presents a relaxation model for the dissipation of a breaking periodic wave. For irregular waves, Dally (1992) applied this approach on a wave-by-wave basis. Rattanapitikon and Shibayama (1998a,b) and Rattanapitikon et al. (2003b) propose estimating the wave energy as $E = \rho g H_{rms}^2/8$ and using a Miche-type criterion for estimating H_{stable} to define $E_{stable} = \rho g H_{stable}^2/8$. We subsequently refer to this model as the D85 dissipation model and use the constant breaking criterion for a stable root-mean-square wave height ($\gamma_D = H_{rms,st}/d = 0.266$) given by Rattanapitikon (2007).

In summary, 12 formulations are considered in the model comparison. These formulations are described in greater detail in Appendix A.

3.2. Depth-induced wave breaking observations

3.2.1. Laboratory observations

To represent a large range of wave conditions, eight data sets with observations made in 1D wave flumes with waves propagating (with two exceptions) over a constant slope were used (see Fig. 2). Occasionally, we used the nominal incident spectrum, either uni-modal or bi-modal, but where available we used the observed incident spectrum. A $\cos^m(\theta)$ directional distribution with $m = 800$ (i.e., directional spreading $\sigma_\theta = 2^0$; Kuik et al., 1988) was used to characterize the long-crested waves.

To avoid redundancy and for reasons of economy, we select from each of the two large data sets of Wallingford (Coates et al., 1998; Hawkes et al., 1998; van der Meer et al., 2000) and Jensen (2002), each with 210 and 110 cases respectively, a representative sample. It comprised of (a) the cases closest to the central values of the experimental parameters (the significant wave height, mean wave period, spectral shape, etc.), (b) the cases at the extreme values of these parameters (representing the envelope) and (c) a random sample of 25 remaining cases. This resulted in 49 Wallingford cases and 45 Jensen (2002) cases. For the Wallingford data set, the observations are divided into two data sets; one containing observations on the slope and the other over the horizontal flat resulting in 98 cases. The remaining six laboratory data sets are included in their entirety.

3.2.2. Idealized field observations

To include observations representing wave generation limited by depth-induced wave breaking, we include observations from three shallow lakes (see Fig. 3): Lake George in south–east Australia (Young and Babanin, 2006) and Lake IJssel and Lake Sloten in the Netherlands (Bottema and van Vledder, 2009). These authors presented their observations as dimensionless energy $\tilde{E} = g^2 m_0/U_{10}^4$ as a function of dimensionless depth $\tilde{d} = g\ d/U_{10}^2$, in which U_{10} is the average wind speed at 10 m elevation implying an idealization of depth, fetch and wind, i.e., fully developed waves in shallow water.

From these lakes, we selected data points representing the upper envelope of the dimensionless energy $\tilde{E}$ when plotted against $\tilde{d}$ (see inset of Fig. 1 in Supplementary Materials) but only in the range where depth-induced breaking dominates (approximately $\tilde{d} < 0.05$; verified with SWAN computations). In the computations, these cases are treated as idealized 1D cases with constant wind and water depth. As the exact wind speed is immaterial for dimensionless quantities, a wind speed of 20 m/s was used.

3.2.3. Coastal field observations

Finally, we consider four coastal sites of increasing complexity (see Fig. 4), namely a relative simple, straight, and gently sloping beach open to the sea (Petten), a bay with a large shoal half across its entrance (Haringvliet), a complex inter-tidal region (Amelander Zeegat), and a tropical fringing reef (Guam). In these cases, the wave boundary conditions are 2D spectra inferred from directional wave buoys in deep water. Wave induced set-up is computed with linear wave theory but without calculating wave-induced currents for all but one field case. This is used for Petten, Haringvliet and Guam for which we estimate the current speed < 0.25 m/s (based on observations and tide tables). For Amelander Zeegat, a separate circulation model was used to compute the wind, the wave and tide induced currents, and the wind and wave induced set-up (van der Westhuysen and de Waal, 2008). The wind and tide induced currents and water levels were computed with the same circulation model for Petten (Groeneweg et al., 2003; G.Ph. van Vledder, pers. comm., 2012).

To avoid observations insensitive to depth-induced breaking, only locations demonstrating a 5% variation in the SWAN computed significant wave height between $\gamma_{BJ} = 0.73$ and $\gamma_{BJ} = 1.5$ were considered. Using the latter value essentially disables wave breaking. At the Haringvliet site, this removed all observations in depths >10 m, while at the Petten site only some of the observations were removed. All other field cases are included in their entirety.

3.2.4. Calibration and validation subsets

For the model comparison in Section 5, all 225 cases from the 13 data sets were used. This includes 202 laboratory cases, 5 lake cases and 18 coastal cases. For the calibration and verification of our joint scaling in Section 6, we split the 225 cases into two mutually exclusive subsets respectively. For the first set (the calibration subset), we used a subset of Wallingford and of Jensen (2002) representing the central and envelope cases i.e., criteria (a) and (b). Similar criteria were also used to add 1:100 and 1:250 slope cases from Katsardi et al. (2013) to increase the range of slopes in the calibration. These criteria ensured that the calibration subset

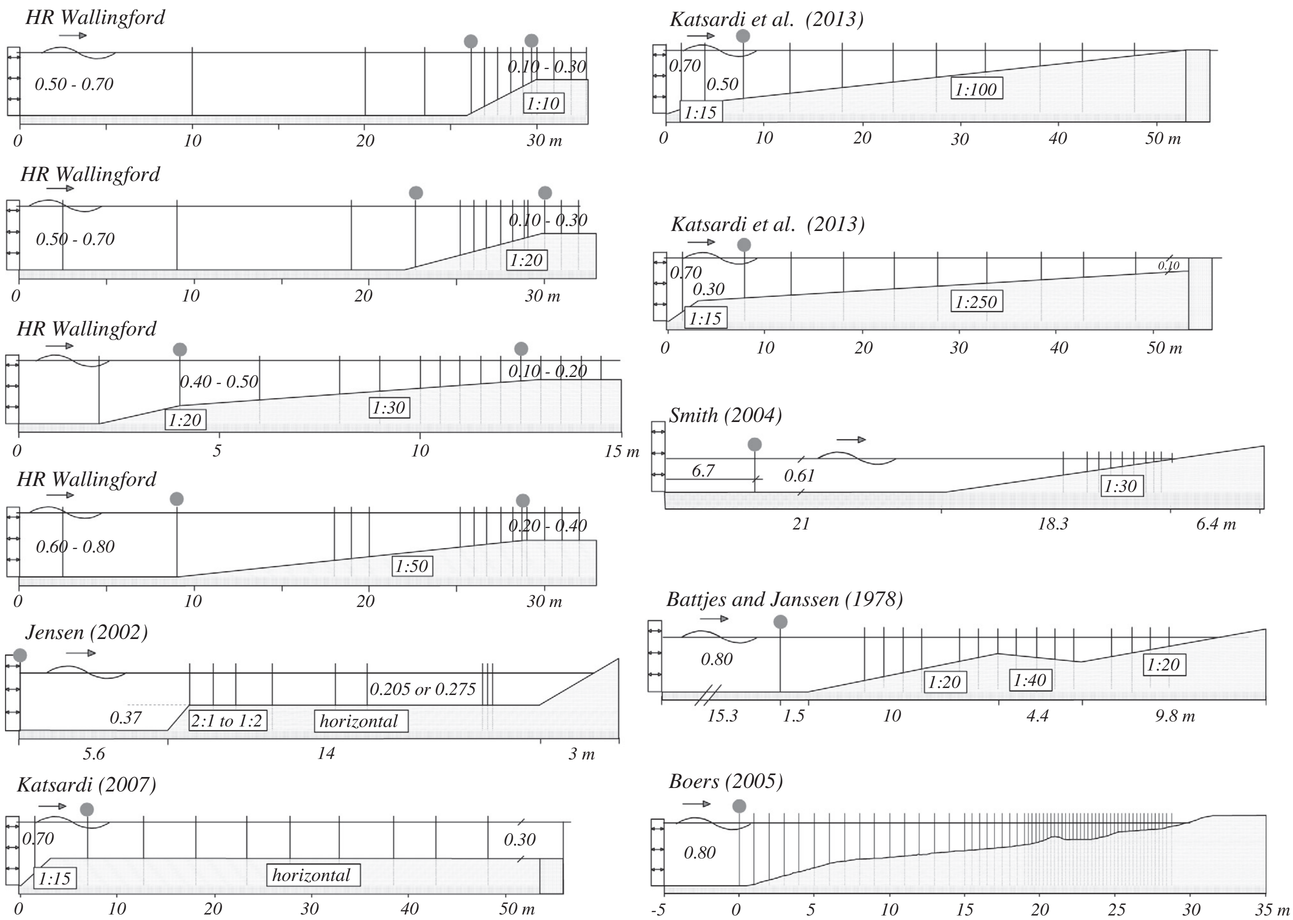

Fig. 2. The configurations of the laboratory observations. Thin vertical lines indicate wave gauge positions. Solid dots indicate the location of incident spectra for the computations (wave boundary condition).

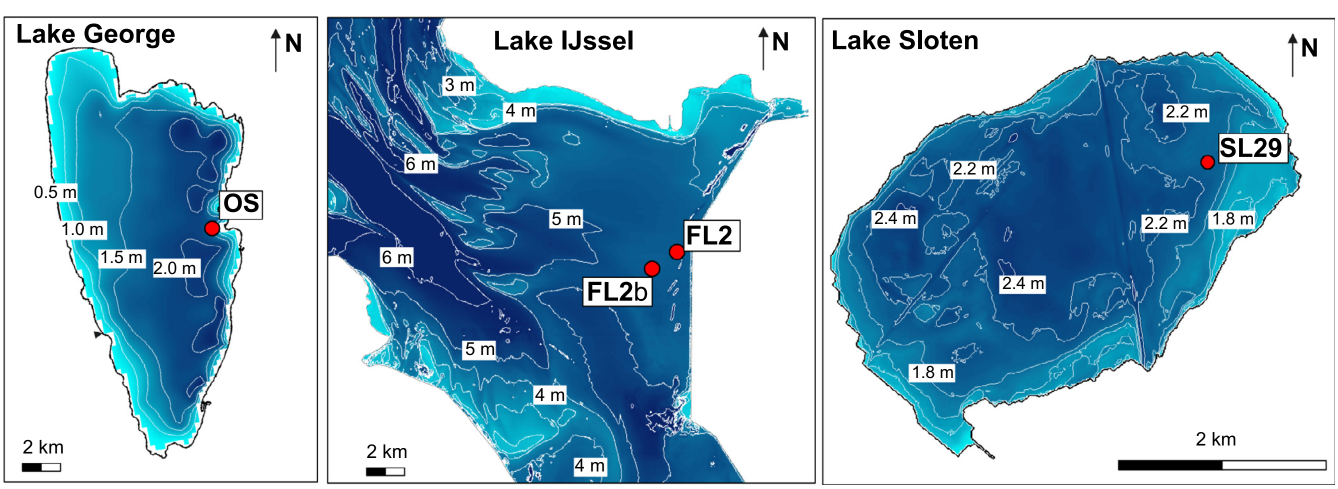

Fig. 3. The bathymetry of the three lakes with the location of observation sites OS, FL2, FL2b and SL29.

remained as unbiased as possible to specific experimental parameters. To represent locally generated waves, the lakes data set was also added in its entirety. In total, for the calibration, 84 1D cases were used i.e., 48 from Wallingford, 20 from Jensen (2002), 11 from Katsardi et al. (2013) and 5 from the lakes data set.

For the second set (the verification subset), all remaining laboratory cases were used and all field cases (except the lakes). This included the randomly selected cases from Wallingford and Jensen (2002), the remaining (outside the calibration subset) 12 cases from Katsardi et al. (2013) and Katsardi (2007) and all remaining laboratory data sets, totaling 123 cases. The addition of the 18 field cases brought the total number of verification cases to 141. Further details of all cases are provided in Supplementary Materials.

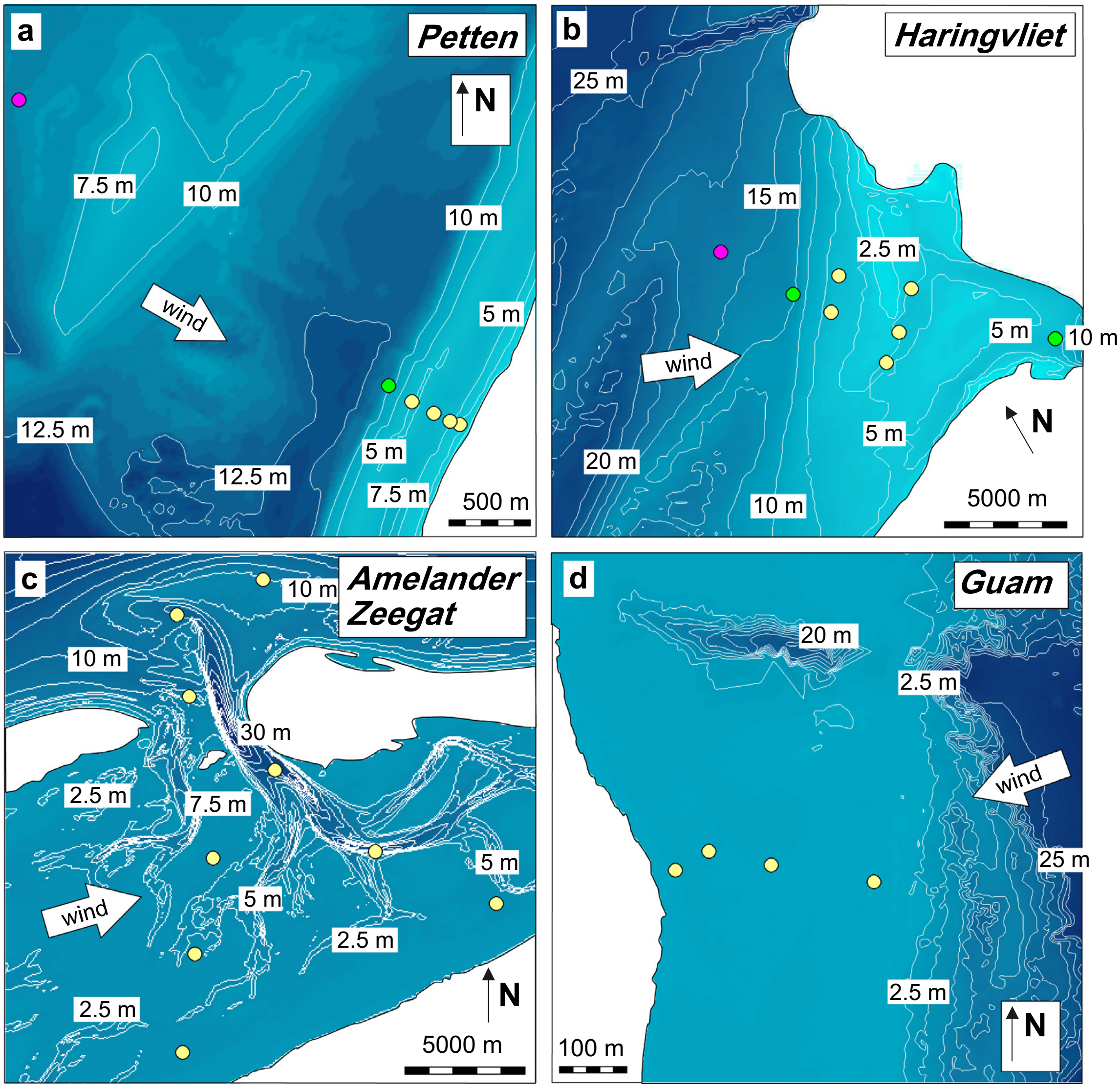

Fig. 4. The bathymetry of the coastal sites Petten, Haringvliet, Amelander Zeegat and Guam. Water depth for mean sea surface at +1 m above chart datum (Amsterdam Ordnance Datum for Petten, Haringvliet and Amelander Zeegat, and mean lower low water for Guam). The buoy locations are indicated by colored dots: purple (boundary condition), green (occasionally removed when not affected by depth-induced breaking) and yellow (always affected by depth-induced breaking). The indicated wind directions are the average direction over the cases per site (variation over the different cases < 35° for Petten ,<20° for Amelander Zeegat, and <25° for Guam). The wind direction did not vary significantly for the Haringvliet site. (For interpretation of the references to color in this figure legend, the reader is referred to the web version of this article.)

3.3. Method of analysis

For our analysis, the errors in the prediction of the significant wave height are expressed in terms of a scatter index (*s.i.*) and a relative bias (*rel.bias*) as used in previous studies (e.g. Janssen et al., 1984; Komen et al., 1994; van der Westhuysen, 2010). They are defined here as:

$$s.i. = \sqrt{\frac{1}{N}\sum (H_{m0,\,comp} - H_{m0,\,obs})^2} \Big/ \bar{H}_{m0,\,obs} \tag{3}$$

$$rel.bias = \frac{1}{N}\sum (H_{m0,\,comp} - H_{m0,\,obs}) \Big/ \bar{H}_{m0,\,obs} \tag{4}$$

The subscripts *obs* and *comp* refer to the observed and computed values, N is the number of data points and the overbar indicates the mean value. We use these metrics only to indicate the magnitude of the errors.

To determine characteristic averages of these metrics, we divided the data sets into cases with sloping profiles; typically well predicted in the literature and those with horizontal profiles; typically poorly predicted. The distinction is evident in all cases except the Guam reef. The Guam reef is often assumed to be horizontal with a fairly steep approach slope (e.g. Demirbilek et al., 2007), but actually the slope is 1:700 and negative with most of the wave breaking occurring over an elevated threshold at the deep water edge. Nevertheless, we consider 1:700 gentle enough to be included in the horizontal subset. Furthermore, we also make the distinction between laboratory and field cases.

For each subset (slopes, horizontals, laboratory and field), we compute the metrics for each individual data set and compute the average, unweighted by the number of cases in each sample data set to avoid biasing towards large sample data sets. The overall average is the unweighted average of the sloping and horizontal subsets. We consider the scatter index to be the primary metric to assess performance as it includes the systematic and random error of the prediction. The relative bias represents only the systematic error.

4. New parameterizations

4.1. A joint scaling for depth-induced wave breaking

4.1.1. The $\beta - kd$ scaling

Following the depth-induced wave breaking models outlined in Section 3.1, we propose a joint scaling dependent on both local bottom slope, β and local normalized characteristic wave number, $\tilde{k}d$ (see Section 4.1.2). In very shallow water ($\tilde{k}d \to 0$), waves behavior converges to that of a solitary wave. Theoretically, the wavelength of such waves is infinitely long and therefore wavelength, and therefore the value of $\tilde{k}d$ becomes less and less relevant as waves propagate into shallower water. For instance, Fenton (1990, his Fig. 6-1) shows that for such waves, the maximum wave height and therefore γ is virtually independent of $\tilde{k}d$. We therefore argue that at some lower limit for $\tilde{k}d$ (to be determined through calibration), wave breaking is only controlled by β. At larger $\tilde{k}d$ values, waves are assumed to be dependent on both β and $\tilde{k}d$. To accommodate this, we represent the two different dependencies on local bottom slope and normalized wave number, respectively, as linear scalings, equivalent to those proposed in previous studies, with $\gamma_1(\beta) = \gamma_0 + a_1 \tan\beta > 0$ and $\gamma_2(\tilde{k}d) = a_2 + a_3\tilde{k}d \geqslant 0$ where γ_0, a_1, a_2 and a_3 are tunable coefficients. To provide a smooth transition from the linear dependency on the local normalized wave number in deep water ($\tilde{k}d > 1$) to a linear dependency on the local bottom slope in shallower water ($\tilde{k}d < 1$), we introduce a hyperbolic tangent:

$$\gamma_{\beta-kd} = \gamma_1(\beta)/\tanh[\gamma_1(\beta)/\gamma_2(\tilde{k}d)] \tag{5}$$

As wave progress into shallower water, $\tilde{k}d \to 0$ and the proposed scaling for gamma converges to a linear dependency only dependent on β i.e., $\gamma_{\beta-kd} \to \gamma_1(\beta)$. In deeper water, $\tilde{k}d \to \infty$ and $\gamma_{\beta-kd} \to \gamma_2(\tilde{k}d)$. The $\tilde{k}d$ range between these two extremes is determined by the coefficients a_2 and a_3. We refer to this joint scaling as the $\beta - kd$ scaling.

The bottom slope in Eq. (5) is (implicitly) assumed to be positive, i.e., decreasing depth in the mean wave direction. In arbitrary and naturally occurring 2D bathymetries, backwards or sideways sloping profiles (relative to the mean wave direction) occur. As we do not have a rationale for estimating γ under such conditions, we estimate the bottom slope as the magnitude of the bottom gradient taken from the computational grid i.e., $\tan\beta = |\nabla d|$, thus not discriminating between forward, backward or sideways sloping profiles. Whitford (1988, p. 110) supports this to some extent through his observations of H_{rms}/d as a function of $\tan\beta$ in a saturated surf zone where he shows the observations to cluster around a common regression line, with the same degree of scatter, for both positive and negative slopes. Our approach also avoids estimating bottom slopes as horizontal in the mean wave direction when that direction is parallel to the depth contours of a sideways sloping bathymetry. In such a situation, the bottom slope in the mean wave direction would be zero, although approximately half the wave energy would be propagating up-slope and the other half down-slope. It is noteworthy however that in trial computations with negative slopes (Boers, 2005 and Guam cases; see Section 6.3), a high local value of $\gamma_{BJ} \sim O(1)$ for negative slopes reduced errors. Furthermore, to prevent physically unrealistic values of $\gamma_1(\beta)$ over very steep slopes, an upper limit of $n = \tan^{-1}(\beta) = 10$, i.e. a limiting 1:10 slope is imposed.

4.1.2. Characteristic wave number

Often in modeling wave breaking, the characteristic wave number is taken at the peak of a typically uni-modal spectrum. However, this is not very robust in arbitrary conditions. Its value tends to behave erratically when small variations in a multi-modal spectrum randomly shift the peak from one frequency to another, in particular off an oceanic coast where the spectrum will generally have multiple peaks due to the presence of multiple swell fields. Using a higher-order mean wave number is also not robust. It is sensitive to the exact shape of the high-frequency tail of the spectrum which spectral wave models cannot accurately predict in very shallow water as triad wave–wave interactions – which tend to generate high-frequency peaks – are poorly accounted for, if at all. We therefore propose using a lower-order mean wave number, as used for white capping (WAMDI group, 1988) $\tilde{k} = k_{-1/2} = \left[\iint k^{-1/2} E(\sigma\theta) d\theta / E\right]^{-2}$. This is less sensitive to the presence of multiple peaks or to the exact shape of the spectral tail.

4.1.3. Calibration

The dependency of $\gamma_{\beta-kd}$ on normalized *wave number* is most evident when the *bottom slope* is zero as under such conditions Eq. (5) reduces to $\gamma_{\beta-kd} = \gamma_0/\tanh[\gamma_0/(a_2 + a_3\tilde{k}d)]$. For the calibration of γ_0, a_2 and a_3, we therefore use horizontal profile cases with a wide $\tilde{k}d$ range; namely the Wallingford and Jensen (2002) calibration subsets with $0.4 \leqslant \tilde{k}d \leqslant 1.1$ and $0.5 \leqslant \tilde{k}d \leqslant 1.0$ respectively and the lakes data set with $1.1 \leqslant \tilde{k}d \leqslant 1.4$. However, in the first two (low $\tilde{k}d$, laboratory) data sets a few dozen cases are available whereas in the third (high $\tilde{k}d$, lakes) data set only five cases are available. A calibration using all three data sets simultaneously would therefore be seriously biased towards the lower $\tilde{k}d$ values. To avoid this, we follow van der Westhuysen (2010, his Fig. 7) to estimate the optimal $\gamma_{\beta-kd}$ value for the high $\tilde{k}d$ data set by calibrating $\gamma_{\beta-kd}$ independently from β or $\tilde{k}d$. This calibration consisted of systematically varying the value of $\gamma_{\beta-kd}$ in the range $0 < \gamma_{\beta-kd} \leqslant 1.5$ and calculating the corresponding scatter index.

We subsequently calibrate γ_0 and a_2 by systematically varying these coefficients over the low $\tilde{k}d$ data sets. For each $\gamma_0 - a_2$ pair, we calculated the average scatter index by equally weighting Wallingford and Jensen (2002). Applying the optimum value for $\gamma_{\beta-kd}$ at the lower $\tilde{k}d$ limit for the lakes data set allowed a_3 to be determined. Following Roelvink (1993), the optimum combination of γ_0 and a_2 was determined by plotting the isolines of the average scatter index in the $\gamma_0 - a_2$ plane and determining the location of the minimum.

The coefficient for slope dependence, a_1 was calibrated last using the sloping calibration cases of Wallingford and Katsardi et al. (2013) from the equally weighted scatter indices.

4.2. Extension of dissipation models for wave directionality

For waves breaking in a laboratory flume, the 1D bore analogy used in most dissipation models is a reasonable assumption. However, in reality, all waves in the field are essentially short-crested, even if refraction elongates the crests near a straight coastline. Therefore, in these cases, we expect the inherent short-crestedness of the waves to detract from the 1D bore analogy. As a preliminary investigation on the extent of directional effects, we consider a modification for dissipation models to account for the inapplicability of the 1D bore assumption for waves in 2D conditions.

The directional spreading of waves can be defined as the standard deviation of the frequency integrated 2D spectrum (Kuik et al., 1988):

$$\sigma_\theta = 2\left[\int_{\theta_0-\pi}^{\theta_0+\pi} \sin^2\left(\frac{\theta-\theta_0}{2}\right) D(\theta) d\theta\right]^{1/2} \tag{6}$$

in which θ_0 is the mean wave direction and $D(\theta)$ is the direction distribution defined as $D(\theta) = \int E(f,\theta)df/E$.

We assume that the analogy between the dissipation of a 1D breaking bore and a breaking wave holds for long-crested waves i.e., directionally narrow spectra with a directional spreading, $\sigma_\theta < \sigma_\theta^*$ (to be determined later). For more directionally spread spectra ($\sigma_\theta > \sigma_\theta^*$), we assume the same for each partitioning of the spectrum of width σ_θ^*. Such a partitioning can be considered as an expansion of the frequency partitioning of Filipot and Ardhuin (2012). As a step towards a fully 2D frequency and directionally partitioned spectrum and to maintain the simplicity, we only consider a simple directional partitioning by defining the number of partitions as $K_\theta = \sigma_\theta/\sigma_\theta^*$. To implement this, we divide the energy in the dissipation formulations by K_θ (equivalent to $\sqrt{K_\theta}$ for rms-wave height) to represent the energy in each partitioning and multiply the bulk dissipation by K_θ to represent the sum of the dissipation from all the partitions. This implicitly assumes a uniform energy distribution. It should be clear that this is not the same as spectral partitioning of e.g. Hanson and Phillips (2001) who considered a partitioning of the 2D spectrum into different wave systems. This technique can be used for all models based on the 1D bore assumption i.e., BJ78, TG83, B98. To illustrate this, BJ78 (Eqs. (A1) and (A2)) is modified to:

$$\varepsilon_{BJ}^{\theta} = -\frac{1}{4}K_\theta \alpha_{BJ}\bar{f}Q_b\rho g H_{max}^2 \tag{7}$$

with

$$\frac{1-Q_b}{lnQ_b} = -\left(\frac{H_{rms}/\sqrt{K_\theta}}{H_{max}}\right)^2 \tag{8}$$

It is arguable, from a physical perspective, that instead of modifying the dissipation directly, the underlying wave height distribution should be revised or a more rigorous implementation applied. However, here we only explore the limitations of the 1D bore assumption and the possible effects of wave directionality. We discuss the effect of this directional partitioning in Section 7.

5. Comparison of available depth-induced wave breaking models

5.1. Model comparison

The validation metrics are shown for all 12 models and 13 data sets separately in Figs. 5 and 6. The performance of the different models varies widely with individual scatter indices between 2% and 79% with the *overall* scatter index per model varying between

	Scatter index	#	DISSIPATION MODELS + SCALINGS											
			BJ78				TG83					B98		D85
			BJ	Mad'76	Ting'01+	T&M'02	S&Hol'85	S&How'89	Lipp'96+	vdW'09	FA'12	Rue'03		R&S'03/07
SLOPE DATA SETS	Slopes												corrected	
	Wallingford*	49	0.06	0.10	0.11	0.18	0.08	0.13	0.16	0.07	0.06	0.07	0.08	0.06
	Katsardi*	18	0.13	0.14	0.23	0.34	0.16	0.22	0.24	0.15	0.10	0.16	0.17	0.12
	Smith*	31	0.08	0.08	0.13	0.26	0.14	0.22	0.28	0.08	0.11	0.10	0.10	0.09
	Boers*	3	0.05	0.07	0.15	0.41	0.19	0.31	0.36	0.06	0.13	0.11	0.08	0.10
	B-J*	2	0.05	0.13	0.15	0.34	0.13	0.24	0.32	0.06	0.07	0.07	0.07	0.10
	Petten**	8	0.15	0.17	0.19	0.57	0.45	0.53	0.55	0.15	0.23	0.15	0.13	0.15
HORIZONTAL DATA SETS	Horizontal													
	Wallingford*	49	0.07	0.07	0.10	0.29	0.11	0.13	0.13	0.08	0.07	0.07	0.07	0.06
	Katsardi*	5	0.10	0.10	0.11	0.40	0.19	0.26	0.27	0.10	0.03	0.11	0.11	0.10
	Jensen*	45	0.21	0.21	0.37	0.30	0.11	0.14	0.14	0.27	0.21	0.24	0.26	0.26
	AZG**	3	0.16	0.15	0.10	0.58	0.47	0.53	0.55	0.10	0.24	0.15	0.14	0.20
	Lakes**	5	0.16	0.17	0.08	0.64	0.66	0.71	0.71	0.10	0.27	0.02	0.02	0.11
	Guam**	4	0.38	0.29	0.52	0.79	0.41	0.45	0.48	0.56	0.47	0.39	0.29	0.44
	Haringvliet**	3	0.17	0.17	0.37	0.51	0.31	0.56	0.60	0.20	0.12	0.19	0.20	0.14
AVERAGES	Averages													
	slopes	111	0.09	0.12	0.16	0.35	0.19	0.27	0.32	0.10	0.12	0.11	0.10	0.10
	horizontal	114	0.18	0.17	0.24	0.50	0.32	0.40	0.41	0.21	0.20	0.17	0.15	0.19
	laboratory*	202	0.09	0.11	0.17	0.32	0.14	0.20	0.24	0.11	0.10	0.12	0.12	0.11
	field**	23	0.20	0.19	0.25	0.62	0.46	0.55	0.58	0.23	0.27	0.18	0.16	0.21
	overall	225	0.13	0.14	0.20	0.43	0.26	0.33	0.37	0.15	0.16	0.14	0.13	0.14
			s.i.< 0.10		0.10<s.i.<0.20		s.i.>0.20						# 1-7	# 8-12

DISSIPATION MODELS

BJ78 = Battjes & Janssen (1978)
TG83 = Thornton & Guza (1983)
B98 = Baldock et al. (1998)
corrected = correction of B98 by Janssen (2008), Janssen and Battjes (2008) and Alsina and Baldock (2008); Rue model
D85 = Dally et al. (1985)

GAMMA SCALINGS

BJ = γBJ = 0.73 (BJ model)
Mad'76 = Madsen (1976)
Ting'01+ = Ting (2001, present authors)
T&M'02 = Tajima & Madsen (2002)
S&Hol'85 = Sallenger & Holman (1985)
S&How'89 = Sallenger & Howd (1989)
Lipp'96+ = Lippmann et al. (1996, present authors)
vdW'09 = van der Westhuysen (2009)
FA'12 = Filipot & Ardhuin (2012)
Rue'03 = Ruessink et al. (2003)
R&S'03/'07 = Rattanapitikon et al. (2003) + Rattanapitikon [2007]

Fig. 5. Scatter index of the 12 models (columns) based on four different dissipation models for 13 data sets (rows) containing a total of 225 cases consisting of laboratory observations (*) and field observations (**). The highlight colors indicate two classes of performance and three ranges of scatter index. The best performing parameterizations on average (overall scatter index < 20%) are shown in green. The individual performance for each parameterization per data set is indicated in blue for scatter indices < 10%, orange for scatter indices > 20% and blank for values between these two limits. Averaged values as described in Section 3.3 are also provided. (For interpretation of the references to colour in this figure legend, the reader is referred to the web version of this article.)

			DISSIPATION MODELS + SCALINGS											
	Relative bias	#	BJ78				TG83					B98		D85
			BJ	Mad'76	Ting'01+	T&M'02	S&Hol'85	S&How'89	Lipp'96+	vdW'09	FA'12	Rue'03		R&S'03/07
SLOPE DATA SETS	Slopes												corrected	
	Wallingford*	49	0.04	0.08	0.09	-0.15	-0.05	-0.11	-0.14	0.05	0.01	0.05	0.06	0.03
	Katsardi*	18	0.11	0.13	0.22	-0.29	-0.08	-0.16	-0.19	0.13	0.07	0.14	0.15	0.06
	Smith*	31	0.00	0.06	0.03	-0.22	-0.11	-0.18	-0.24	0.02	-0.05	0.00	0.04	0.01
	Boers*	3	-0.02	0.05	-0.01	-0.39	-0.17	-0.28	-0.34	0.00	-0.09	-0.07	-0.01	-0.08
	B-J*	2	0.00	0.11	0.12	-0.31	-0.11	-0.22	-0.30	0.03	-0.03	0.01	0.03	0.05
	Petten**	8	0.01	0.03	0.06	-0.17	-0.09	-0.13	-0.15	0.02	-0.02	0.01	0.02	0.00
HORIZONTAL DATA SETS	Horizontal													
	Wallingford*	49	0.04	0.06	0.07	-0.24	-0.08	-0.12	-0.14	0.05	0.02	0.03	0.05	0.01
	Katsardi*	5	0.09	0.09	0.10	-0.40	-0.19	-0.25	-0.27	0.10	0.02	0.10	0.10	0.09
	Jensen*	45	0.17	0.18	0.33	-0.29	0.00	-0.04	-0.05	0.23	0.16	0.21	0.22	0.22
	AZG**	3	-0.12	-0.11	0.00	-0.49	-0.41	-0.47	-0.49	-0.06	-0.21	-0.08	-0.08	-0.15
	Lakes**	5	-0.16	-0.17	0.08	-0.63	-0.64	-0.69	-0.70	-0.10	-0.27	0.01	0.01	-0.11
	Guam**	4	-0.21	-0.02	-0.38	-0.69	-0.31	-0.37	-0.40	-0.46	-0.25	-0.25	-0.12	-0.33
	Haringvliet**	3	0.14	0.14	0.33	-0.44	-0.26	-0.49	-0.53	0.18	-0.05	0.15	0.17	0.11
AVERAGES	Averages													
	slopes	111	0.02	0.07	0.09	-0.25	-0.10	-0.18	-0.23	0.04	-0.02	0.02	0.05	0.01
	horizontal	114	-0.01	0.02	0.08	-0.45	-0.27	-0.35	-0.37	-0.01	-0.08	0.02	0.05	-0.02
	laboratory*	202	0.05	0.09	0.12	-0.28	-0.10	-0.17	-0.21	0.08	0.02	0.06	0.08	0.05
	field**	23	-0.07	-0.02	0.02	-0.49	-0.34	-0.43	-0.45	-0.08	-0.16	-0.03	0.00	-0.09
	overall	225	0.01	0.05	0.08	-0.35	-0.19	-0.26	-0.30	0.02	-0.05	0.02	0.05	0.00
			rel. bias > 0	rel. bias < 0									# 1-7	# 8-12

Fig. 6. Same as Fig. 5 for the relative bias. Highlights indicate positive (light blue) and negative or ∼ zero (dark blue) bias over horizontal bathymetries for the cluster of seven best performing models. (For interpretation of the references to color in this figure legend, the reader is referred to the web version of this article.)

13% and 43%. The scatter index for the seven best performing models (indicated with green highlights in Fig. 5) clusters around 14%. This result agrees with Apotsos et al. (2008) who demonstrates errors between 10% and 20% and concludes that no default (or tuned) model provides the best prediction for their observations. This relatively small error is mostly due to a very good performance over the sloping laboratory cases (typically scatter indices < 10%), combined with a reasonable performance in the field cases except the Guam reef.

The correction to the B98 model (e.g. Janssen, 2006) is shown to have only a marginal effect on the performance. The *kd*-scaling from Ting (2001) performs slightly worse with an overall scatter index ∼20% and demonstrates a particularly poor performance for non-locally generated waves over a (near) horizontal bathymetry (the Haringvliet; Jensen, 2002 and Guam cases). The performance of the remaining five models vary from reasonable in some laboratory cases to poor in the field cases where scatter indices are typically ∼50% or higher.

Concentrating on the seven best performing models with rms-errors ∼14%, shows that the largest errors occur in the cases with *horizontal* bathymetries where the highest overall scatter index per model varies between 29% and 56% compared with 15% and 23% for sloping bathymetries. Over horizontal bathymetries, the errors are mostly systematic as shown by the relative bias in Fig. 6, of which the average absolute value is 0.72 times the average scatter index.

5.2. Correlation with bottom slope and normalized wave number

To find a possible cause for the errors, we plot the scatter index and the relative bias of the seven best performing models in Fig. 7. These models are not individually indicated, except the BJ model and the best overall performing model; the corrected B98 model with the scaling of Ruessink et al. (2003) (subsequently referred to as the Rue model) as references. For the sloped bottom data sets (Fig. 7(a)), the bias is only weakly correlated with the scatter index. In the horizontal bottom data sets (Fig. 7(b)), the Guam data set is obviously an outlier with high scatter indices, however as discussed previously, its classification is questionable. If therefore, for this analysis, we ignore the Guam data set, we see that in contrast to the slope data sets, for the horizontal cases, the bias is highly correlated with the scatter index. In addition, there is a sharp distinction between data sets with a negative or ∼ zero bias (under-prediction of locally generated waves in the lakes and the Amelander Zeegat) and with a positive bias (over-prediction of non-locally generated waves in the Wallingford; Katsardi, 2007; Jensen, 2002 and Haringvliet data sets).

Typically for locally generated wave cases, the relative bias is on average ∼64% (negative) of the total error suggesting a severe systematic under-prediction in agreement with previous studies (e.g. van der Westhuysen, 2010). In cases of finite depth wave growth, models with either a direct dependency on the normalized wave number (*kd*; Ting, 2001; Ruessink et al., 2003) or indirect (van der Westhuysen, 2009, 2010; through the Ursell number) perform significantly better with averaged scatter indices typically half those from models without such a dependency. However, none of these models provide the smallest errors for both Amelander Zeegat and the lakes.

A similar analysis for non-locally generated wave cases show a severe over-prediction of significant wave heights with larger errors for horizontal bathymetries (∼73% of the mean bias) than for sloping bathymetries (∼28% of the mean bias). This is in agreement with Nelson (1997) and Katsardi (2007) who both demonstrate higher dissipation for wave breaking over horizontal bathymetries than over sloping bathymetries.

These contrasts support a joint dependency on both local bottom slope (shown by the contrast in horizontal and sloping

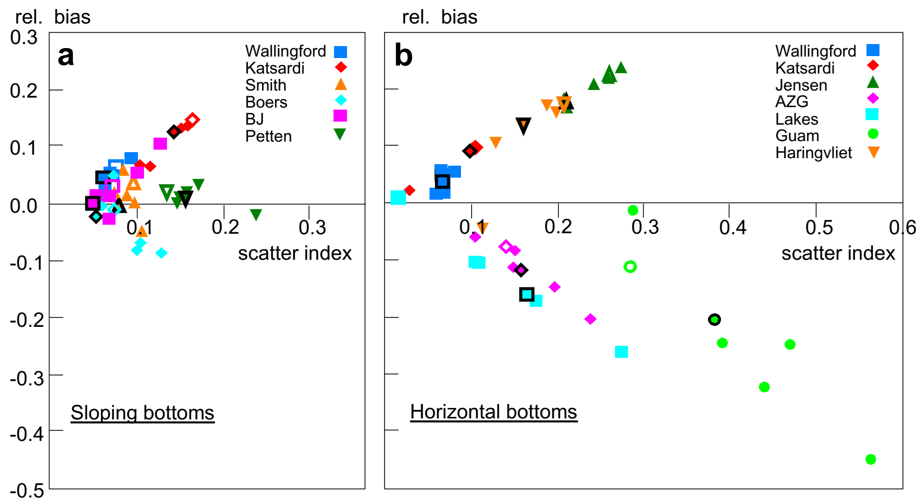

Fig. 7. The scatter diagram of the relative bias versus the scatter index for all data sets and the cluster of seven best performing models (not identified individually). The reference BJ model is shown with a solid black outline and the reference Rue model is shown with only a symbol outline. The Amelander Zeegat data set is indicated with AZG and the Battjes and Janssen (1978) data set with BJ.

bathymetries for non-locally generated waves) and on normalized wave number (shown by the contrast in locally and non-locally generated waves over horizontal bathymetries). Such joint dependencies have been considered before (e.g. Goda, 2004, 2009, 2010; Raubenheimer et al., 1996), however these are not applicable for use in 2D spectral wave models (see Section 3.1).

6. Calibration and verification of the $\beta - kd$ scaling

6.1. Dissipation model

Following the model comparison, it is clear from Fig. 5 that the simplest dissipation models with constant γ (the BJ and the D85 model with $\gamma_{DDD} = 0.266$), in terms of overall scatter index, are among the best performing models and occasionally perform slightly better than the more complex models of van der Westhuysen (2009) and Filipot and Ardhuin (2012). Following these observations, in addition to its proven robustness (Battjes and Janssen, 2008), we choose to address the scaling of the BJ78 dissipation model. Other alternatives may have a better foundation in physics, particularly in regards to the assumed statistical distribution of the wave heights, but we agree with Battjes and Janssen (1978) that the details of the distribution are not important when only integral parameters are required.

6.2. Calibration

Using our calibration procedure in Section 4.1.3, the four calibration parameters of the $\beta - kd$ scaling ($\gamma_0, \alpha_1, \alpha_2$ and α_3) were calibrated over the calibration subset. For the high $\tilde{k}d$ cases (lakes data set), we present our calibration for $\gamma_{\beta-kd}$ (independent of β and kd) in Fig. 8(a). These results agree with van der Westhuysen (2010) and demonstrate a sharp decrease in the scatter index from ~100% to an asymptote at ~5% for $\gamma_{\beta-kd} \geqslant 0.95$.

Using this limit so that $\gamma_{\beta-kd} = 0.95$ for $\beta = 0$ and $\tilde{k}d = 1.1$ (assumed to be the limit between high and low $\tilde{k}d$), a_3 was determined for each $\gamma_0 - a_2$ pair. From the average scatter indices over the horizontal Wallingford and Jensen (2002) calibration subsets, an error contour plot is shown in Fig. 8(b). The relatively flat error gradient in the a_2 axis compared to the γ_0 axis demonstrates a sensitivity on γ_0 rather than a_2 for low $\tilde{k}d$ cases over horizontal bathymetries. For these conditions, a minimum error of ~6%, was achieved with $\gamma_0 = 0.54$ and $a_2 = -8.06$ (so that $a_3 = 8.09$). This

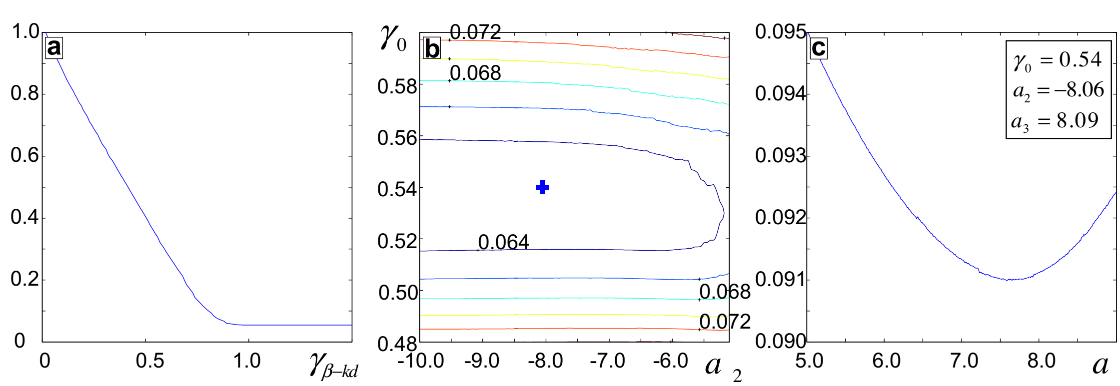

Fig. 8. Variation of the scatter index for significant wave height during calibration. Shown are (a) scatter index using a fixed $\gamma_{\beta-kd}$ per computation in the lakes data set, (b) isolines of scatter index for the calibration of γ_0 and a_2 in the horizontal bottom calibration cases of Wallingford and Jensen (2002) (minima denoted by the blue cross) with $\gamma_{\beta-kd} = 0.95$ for $\tilde{k}d = 1.1$ and (c) scatter index for the calibration of a_1 in the sloping bottom calibration cases of Wallingford and Katsardi et al. (2013) with $\gamma_0 = 0.54$, $a_2 = -8.06$ and $a_3 = 8.09$. (For interpretation of the references to colour in this figure legend, the reader is referred to the web version of this article.)

lower limit, γ_0, is identical to the value found by Katsardi (2007) through numerical experiments and similar to the observations of Nelson, 1997; $\gamma_0 = 0.55$). The calibration coefficient a_2 defines the lower limit of $\tilde{k}d$ dependency which, from calibration, is given at $\tilde{k}d \approx 1$. This is consistent with van der Westhuysen (2010, his Fig. 7) who demonstrates $\gamma_{BJ} > \gamma_0$ for horizontal cases over deep water depths ($\tilde{k}d > 1$).

Finally, a_1, the bottom slope dependency coefficient is calibrated from the sloping bottom calibration subsets of Wallingford and Katsardi et al. (2013). This is shown in Fig. 8(c) with a well-defined minimum at $a_1 = 7.59$ and averaged error of $\sim$9%. This positive β−variation is consistent with the $\gamma(\beta)$ scalings considered in the model comparison, however for the $\beta - kd$ scaling the variation of γ with β is stronger. This is needed to account for a wider range of γ-values given by the lower limit γ_0. The commonly used value $\gamma_{BJ} = 0.73$ is reproduced for slopes of 1:40 in shallow to intermediate water depths. The fully calibrated $\beta - kd$ scaling is shown in Fig. 9.

6.3. Verification

To verify the performance of the calibrated $\beta - kd$ scaling ($\gamma_0 = 0.54$, $a_1 = 7.59$, $a_2 = -8.06$ and $a_3 = 8.09$), we show our results over the verification subset as described in Section 3.2 in Figs. 10 and 11. The BJ and Rue models are also shown as references representing, respectively, the most common parameterization used in most wave models and the best performing published parameterization.

The overall performance of the $\beta - kd$ scaling for 1D laboratory cases (scatter index = 9%) is slightly better than for the BJ or Rue models (10% and 12%, respectively). Although this improvement appears insignificant, it is biased by the sloping bottom cases where there is no significant overall improvements with average errors of the models in the range $8\% \leqslant s.i. \leqslant 10\%$, implying that the horizontal bottom cases are improved considerably (in fact from $\sim$14% to 7%).

For the gentle slopes of Katsardi et al. (2013) and steeper slopes of Smith (2004), we see modest error reductions, from $\sim$14% to 12% and $\sim$9% to 7%, respectively, with the $\beta - kd$ scaling. However, this is equally diminished by the performance over the remaining sloping bottom cases, particularly over those exhibiting barred beach profiles, i.e., errors increase from $\sim$6% for both the Boers (2005) and Battjes and Janssen (1978) data sets to 7% and 10%, respectively. A possible reason may lie in the treatment of negative slopes (see Section 4.1.1).

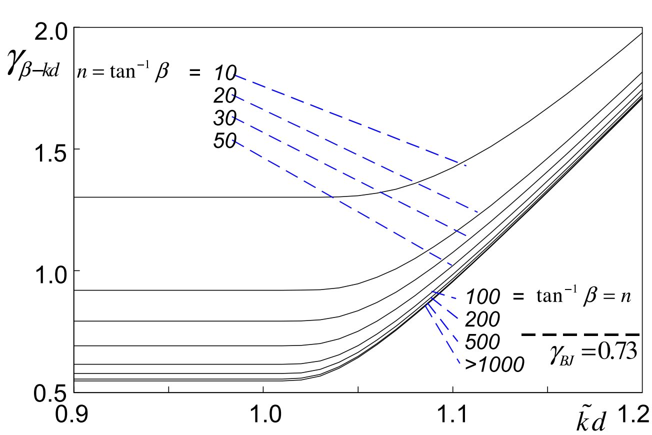

Fig. 9. Calibrated $\gamma_{\beta-kd}$ as a function of bottom slope $n = tan^{-1}\beta$ and normalized characteristic wave number $\tilde{k}d$ and $\gamma_{BJ} = 0.73$ for reference.

The improvements for the horizontal laboratory cases are illustrated by significant error reductions of almost 50%. For these cases, by using the $\beta - kd$ scaling the average scatter index fell to 7% from 13% and 15% when using the BJ and Rue models respectively. Most of this improvement comes from error reductions in Jensen (2002) and Katsardi (2007) data sets with decreases of $\sim$23% to 8% and $\sim$10% to 5%.

It is encouraging to note that over the lakes data set, the calibrated $\beta - kd$ scaling gives significantly smaller errors compared to the BJ model with an error reduction from 16% to 2%. This result is comparable to the performance of the Rue model. The performance of the $\beta - kd$ scaling compared to the lake observations is illustrated in the inset of Fig. 1 in Supplementary Materials.

In the field cases, the averaged performance of the $\beta - kd$ scaling is shown to be similar to the reference BJ and Rue models with average errors in the range $19\% \leqslant s.i. \leqslant 22\%$. The $\beta - kd$ scaling performs better for Guam and Haringvliet with error reductions from 38% (BJ) and 29% (Rue) to 28% and 17% (BJ) and 20% (Rue) to 16% respectively. However, it performs worse for both the sloping Petten and horizontal Amelander Zeegat data sets. In these cases, error increase from $\sim$14% to 20% and $\sim$15% to 23%, respectively.

7. Discussion

The proposed $\beta - kd$ scaling is shown to provide a simple parameterization which improves the modeling skill for the significant wave height over 1D conditions. In particular, it performs well for both locally and non-locally generated waves while being consistent with parameterizations and limits for γ found from previous studies.

The effect of the $\beta - kd$ scaling is twofold. The effect of the bottom slope (i.e., β-) scaling is to shift from a fixed scaling, i.e., $\gamma_{\beta-kd} = 0.73$ to a value varying between $\gamma_{\beta-kd} = 0.54$ and $\gamma_{\beta-kd} = 1.30$ whereas the effect of the wavenumber (i.e., $\tilde{k}d$-) scaling is to always increase $\gamma_{\beta-kd}$ with increasing $\tilde{k}d$ in intermediate water ($\tilde{k}d >\sim 1$) with no upper limit (until white capping becomes dominant). The physical interpretation of this $\tilde{k}d$-scaling is that it accounts for the inherent differences between non-locally and locally generated waves. For waves arriving from a distant source, for example swell waves at a reef, $\tilde{k}d <\sim 1$, the waves may be seen as analogous to solitary waves, which are independent of k, and therefore as $\tilde{k}d \rightarrow 0$, $\gamma_{\beta-kd} \rightarrow \gamma_\beta$. For waves locally generated by wind, for example over a lake or tidal flat, $\tilde{k}d >\sim 1$ which corresponds to a relatively high normalized water depth (or wave number). Under these conditions, wind may *indirectly* impact depth-induced wave breaking by changing the spectral shape and therefore the value for $\tilde{k}d$. However, the time scales of these variations are likely to be too short to have a significant impact on depth-induced wave breaking. The physical relevance of the increasing $\gamma_{\beta-kd}$ is to essentially disable depth-induced dissipation in deep water. Of course under such conditions, steepness-induced breaking (white capping) will still continue to limit the wave heights. Therefore under these conditions the impact of wind (the root cause of white capping) cannot be ignored at shallow and intermediate water depths.

The joint scaling encapsulates two different scales for wave breaking. Over relatively shallow water depths where $\tilde{k}d <\sim 1$ e.g. laboratory experiments and near the coast ($d \approx H$), waves will typically be influenced by bathymetric features and therefore the local bottom slope is important. Over locations with greater depth e.g. some distance from the coast ($d \gg H$), waves are less influ-

			WAVE BREAKING PARAMETERIZATION					
	Scatter index	**#**	BJ	Rue	$\beta - kd$		BJ	Rue
			no correction			$\sigma_\theta^* = 15^o$	$\sigma_\theta^* = 25^o$	$\sigma_\theta^* = 25^o$
SLOPE DATA SETS	**Slopes**							
	Wallingford*	25	0.08	0.09	0.11	(0.11)	(0.08)	(0.09)
	Katsardi*	7	0.14	0.15	0.12	(0.12)	(0.14)	(0.15)
	Smith*	31	0.08	0.10	0.07	(0.07)	(0.08)	(0.10)
	Boers*	3	0.05	0.07	0.07	(0.07)	(0.05)	(0.07)
	B-J*	2	0.05	0.07	0.10	(0.10)	(0.05)	(0.07)
	Petten**	8	0.15	0.13	0.20	0.15	0.15	0.13
HORIZONTAL DATA SETS	**Horizontal**							
	Wallingford*	25	0.08	0.08	0.08	(0.08)	(0.08)	(0.08)
	Katsardi*	5	0.10	0.11	0.05	(0.05)	(0.10)	(0.11)
	Jensen*	25	0.21	0.26	0.08	(0.08)	(0.21)	(0.26)
	AZG**	3	0.16	0.14	0.23	0.08	0.09	0.09
	Guam**	4	0.38	0.29	0.28	0.27	0.36	0.29
	Haringvliet**	3	0.17	0.20	0.16	0.12	0.18	0.21
	Lakes	*5*	*0.16*	*0.02*	*0.02*	*0.05*	*0.12*	*0.05*
AVERAGES	**Averages**							
	slopes	76	0.09	0.10	0.11	0.10	0.09	0.10
	horizontal	65	0.18	0.18	0.15	0.12	0.17	0.17
	laboratory*	123	0.10	0.12	0.09	(0.09)	(0.10)	(0.12)
	field**	18	0.21	0.19	0.22	0.16	0.19	0.18
	overall	141	0.14	0.14	0.13	0.11	0.13	0.14
			s.i.< 0.10		0.10<s.i.<0.20		s.i.>0.20	

Fig. 10. Verification of the $\beta - kd$ scaling in terms of the scatter index with or without optimum σ_θ^*. Performance over laboratory observations (*) and field observations (**) are highlighted in three ranges of scatter index (from blue to orange). The Lakes data set, shown in italic type, is not included in computing the average values (as it is used for calibration) but is shown to demonstrate the effect due to directional spreading for this data set. Laboratory cases with their long-crested waves are unaffected by directional partitioning and are shown within parenthesis () where directional partitioning is used. (For interpretation of the references to colour in this figure legend, the reader is referred to the web version of this article.)

enced by bottom effects. The expected reduction in depth-induced wave breaking is captured by the *kd*− scaling. However, under extreme conditions, such as storms, increased wave heights may occur resulting in a reduction of *kd*. In such conditions, the influence of bottom slope will become important and the scaling of depth-induced breaking will be similar to that found in shallower depths.

However, despite these arguments, for the 2D *field* cases no significant improvements are demonstrated by introducing the $\beta - kd$ scaling. A possible explanation may be in the inherent difference between waves in 1D and 2D conditions. As discussed in Section 4.1.4, the 1D bore analogy is reasonable for laboratory observations. However, for 2D field observations, the inherently short-crested waves are not fully represented by a 1D bore. This discrepancy is most pronounced in the Amelander Zeegat field case where depth-induced refraction causes non-locally generated waves from the North Sea to become focused over and just shoreward of the outer delta. Considering the relative bias for this field case for all the different parameterizations in this study (see Figs. 6 and 11), a distinct negative bias can be seen for virtually all of them. This suggests that as a wave becomes more short-crested, the observed significant wave height increases and therefore the energy dissipation is reduced.

Further support is provided by a number of studies. Babanin et al. (2011) note, in a hindcast of Typhoon Krosa (2007) in shallow water conditions ($H_{m0}/d \approx 0.63$; $d = 38$ m and $H_{m0} \approx 24$ m), that breaking waves from opposite directions resulted in waves much larger than expected on the basis of the BJ model and suggested that this was due to the large directional spreading of the waves. In this situation, the observed wave field consisted of two modes differing 170° in direction, equivalent to directional spreading of $\sigma_\theta \approx 80°$.

However, Dingemans et al. (1986) and Dingemans (1987) report laboratory experiments in a 2D basin showing a weaker effect with smaller directional spreading. We analyzed two cases (case 25 and 28 in Dingemans (1987)) with wave breaking over a horizontal bar with incident JONSWAP spectrum of 0.1 m significant wave height and with a peak period of 0.8 Hz. The bar reduced the water depth from 0.4 m to 0.1 m over the 2 m wide horizontal bar crest (achieved with a 1:20 and 1:10 up- and down-slope, respectively) and caused the waves to break and dissipate. However, increasing the observed directional spreading of the incident spectra from $\sigma_\theta \approx 11°$ to $\sigma_\theta \approx 26°$ (the only difference between the two cases), and corresponding to $\sigma_\theta \approx 8°$ to $\sigma_\theta \approx 20°$ over the top of a bar, resulting in an energy dissipation reduction of only ~5%. Furthermore, Katsardi (2007) and van Vledder et al. (2013) show with numerical models that wave breaking is somewhat affected by the degree of short-crestedness of the waves in shallow water.

These studies suggest that wave directionality enhances the maximum possible breaking wave height in shallow water, but less so as σ_θ reduces. To investigate this, we apply our extension with wave directionality as described in Section 4.2. In Figs. 10 and 11, we show the results for the reference BJ and Rue models and the $\beta - kd$ scaling. For the reference models, $\sigma_\theta^* = 25°$ was used and for the $\beta - kd$ scaling, $\sigma_\theta^* = 15°$. These optimum values were obtained from computations with $\sigma_\theta^* = 10°, 15°, 20°, 25°$ and 30°.

We thus find that the proposed directional partitioning improves all three models for the Amelander Zeegat data set. Errors decrease from 16% and 14% for the BJ and Rue models to 9% for both, and for the $\beta - kd$ scaling, the errors reduce from

			WAVE BREAKING PARAMETERIZATION					
	Relative bias	**#**	BJ	Rue	$\beta - kd$		BJ	Rue
			no correction			$\sigma_\theta^* = 15^o$	$\sigma_\theta^* = 25^o$	$\sigma_\theta^* = 25^o$
SLOPE DATA SETS	**Slopes**							
	Wallingford*	25	0.06	0.07	0.08	(0.08)	(0.06)	(0.07)
	Katsardi*	7	0.12	0.13	0.07	(0.07)	(0.12)	(0.13)
	Smith*	31	0.00	0.04	0.04	(0.04)	(0.00)	(0.04)
	Boers*	3	-0.02	-0.01	-0.04	-(0.04)	-(0.02)	-(0.01)
	B-J*	2	0.00	0.03	0.07	(0.07)	(0.00)	(0.03)
	Petten**	8	0.01	-0.01	-0.07	0.03	0.02	-0.01
HORIZONTAL DATA SETS	**Horizontal**							
	Wallingford*	25	0.04	0.05	-0.01	-(0.01)	(0.04)	(0.05)
	Katsardi*	5	0.09	0.10	0.01	(0.01)	(0.09)	(0.10)
	Jensen*	25	0.18	0.22	0.05	(0.05)	(0.18)	(0.22)
	AZG**	3	-0.12	-0.08	-0.15	-0.04	-0.05	-0.03
	Guam**	4	-0.21	-0.12	-0.03	0.02	-0.19	-0.10
	Haringvliet**	3	0.14	0.17	-0.07	0.09	0.15	0.18
	Lakes	*5*	*-0.16*	*0.01*	*-0.01*	*0.04*	-0.12	0.05
AVERAGES	**Averages**							
	slopes	76	0.03	0.04	0.03	0.04	0.03	0.04
	horizontal	65	0.02	0.06	-0.04	0.02	0.04	0.07
	laboratory*	123	0.06	0.08	0.03	(0.03)	(0.06)	(0.08)
	field**	18	-0.04	-0.01	-0.08	0.02	-0.02	0.01
	overall	141	0.02	0.05	-0.02	0.02	0.03	0.06
			rel. bias > 0.10		rel. bias < 0.10			

Fig. 11. Same as Fig. 10 for relative bias. Highlights indicate positive (light blue) and negative (dark blue) bias for relative biases with magnitudes greater than 10%. A consistent underestimation for field cases is demonstrated with the $\beta - kd$ scaling. (For interpretation of the references to color in this figure legend, the reader is referred to the web version of this article.)

23% to 8%. Almost all of the error reduction is seen in the relative bias which suggests a removal of systematic error. These improvements demonstrate that directional effects, which are not captured by the 1D bore analogy, are significant in complex 2D field cases. In the case of the Amelander Zeegat, over the outer delta, very short-crested waves with $\sigma_\theta >\sim 50^\circ$ occur which are under-predicted by all the models with default settings. By accounting for directional effects, dissipation is reduced for these conditions resulting in a smaller negative bias and improved model performance.

In the remaining field cases (Petten, Haringvliet and Guam), the reference BJ and Rue models are almost insensitive to the directional partitioning whereas some improvements are shown for the $\beta - kd$ scaling. With $\sigma_\theta^* = 15^\circ$, the $\beta - kd$ performs better with an overall average reducing to 11% (from 13%) compared to a mostly unchanged overall average for the reference models of $\sim$14%. From Fig. 11, the decrease in the magnitude of the relative biases (8% to 2% for field cases) demonstrates that the systematic errors are largely removed.

A possible explanation for the insensitivity of the reference models in the remaining field cases may be seen in how these models were calibrated by the original authors. For calibrating these models, field observations are included which may lead to 2D directional effects being implicitly included, i.e., through higher $\gamma-$values. This would then result in larger optimum values for σ_θ^* than if only 1D conditions were considered. In comparison, the $\beta - kd$ scaling is calibrated only over 1D and 1D idealized cases. Therefore, a greater reduction of dissipation is required resulting in a smaller optimum value for σ_θ^*. This provides a consistent explanation for the negative bias seen in the field case verification and the differences over the Petten and Amelander Zeegat cases compared to the reference models.

Wave models are increasingly coupled to circulation models with the resulting radiation stress gradients used to predict wave-induced circulation and set-up. Although much success has been reported in this coupling with wave models where the BJ model is applied (e.g. Dietrich et al., 2013), a number of recent studies have shown this to provide poor modeling skill for currents and set-up. Part of the problem originates from the inflexibility of the BJ model which is constrained to fixed scaling (γ_{BJ}) over the whole domain. For example Mulligan et al. (2010) show the over-prediction of wave breaking and resulting current velocities over the steep slopes of a rocky shoal (foreslope gradient of the shoal is 1:10 over 100 m, and locally 1:1) whereas Lowe et al. (2009a) show improved results over a more gently sloping reef-lagoon system when using lower constant scaling coefficient $\gamma_{BJ} = 0.64$. We expect that our joint parameterization will improved the performance of coupled models to predict wave-induced currents and set-up. Over steep bathymetries, the $\beta - kd$ scaling increases the ratio between the characteristic maximum wave height over local depth with increasing slope which would reduce the over-predictions demonstrated by Mulligan et al. (2010). Over the gentler slopes of the reef-lagoon cases of Lowe et al. (2009a,b), the reef slope was $\sim$1:60. From the $\beta - kd$ scaling, this yields a value of $\gamma_{\beta-kd} \approx 0.67$ for non-locally generated waves (low kd) which is in close agreement with the value used by Lowe et al. (2009a) in their simulations. Further support for the applicability of a lower value for γ_{BJ} in reef cases is shown by the results over the Guam reef cases in Figs. 10 and 11 by the reduced under-estimation over the relatively horizontal bathymetries.

In conclusion, the $\beta - kd$ scaling, while accounting for directional partitioning, provides significant improvements over a wide range of 1D and 2D wave conditions, particularly over horizontal bathymetries. In the laboratory cases, errors are reduced to an average error between 5% and 12% compared to 5% and 21% for the BJ model and 7% and 26% for the Rue model. This improvement demonstrates the applicability of the $\beta - kd$ scaling for non-locally generated 1D cases including significant improvements for observations of wave breaking over horizontal bathymetries. With directional partitioning, improvements are shown for the field cases with the average errors between 8% and 27% compared to 15% and 38% for the BJ model and 13% and 29% for the Rue model. This improvement comes from both the joint scaling and the directional partitioning, particularly over horizontal bathymetries.

The main advantage of the proposed parameterization is that it combines two concepts which have been predominant in the depth-induced wave breaking literature i.e., a dependency on β and a dependency on *kd* in a simple expression. This scaling is consistent with our current physical interpretation for depth-induced breaking. For conditions where *kd* is low, the waves can be considered to converge on solitary wave behavior. The lower limit $\gamma_0 = 0.54$ is consistent with theoretical limits for the crest height of solitary waves (see Appendix A). For high *kd* conditions, the physical interpretation of a reduction of wave non-linearity (e.g. van der Westhuysen, 2010) is also captured by the positive dependency with *kd* which acts to reduce depth-induced breaking. Finally, the directional partitioning provides an adjustment for the 2D nature of 'real' wave fields and is shown to provide improvements for both the proposed joint scaling as well as the reference models.

The implication of this work is that attention is required when developing dissipation models based on the 1D analogy and calibrating over 2D field cases. It may be also noted that similar tendencies have been demonstrated in greater detail for *deep* water waves (e.g. Onarato et al., 2009; Latheef and Swan, 2013) with regards to directionality. Such work may be applicable in our understanding of *shallow* water wave evolution and may potentially result in new source terms which inherently include wave directionality. This work was built upon a large proportion of the parametric wave breaking literature, and although such work can provide useful insights towards wave modeling, future research needs to focus more on third-generation wave modeling i.e., source terms of a non-parametric or first-principles nature, and the detailed balance between the various source terms. With the increased recognition of the importance of breaking waves at the surf zone interface and the increased use of coupled models, better source terms for shallow water wave physics are still needed. Although both the $\beta - kd$ scaling and directional partitioning provide a better parametric representation of this, they are both still heuristic and require further substantiation with theory and empirical evidence.

Acknowledgments

We greatly appreciate receiving the details of the laboratory observations of Jane Smith of the Coastal and Hydraulics Laboratory, US Army Engineer Research and Development Center in Vicksburg (USA). We are equally grateful to the partners of the LOWISH project (Limits on Waves in Shallow Water; a joint initiative project of British Petroleum, Chevron, ConocoPhillips, Shell, Total and Woodside) who provided us with the observations of Imperial College. We thank in particular Kevin Ewans of Shell International Exploration and Production B.V. in The Hague for his assistance and acknowledge with pleasure that these observations were made by Chris Swan and Vanessa Katsardi of Imperial College. The authors also thank Pieter Smit and the anonymous reviewers for their constructive comments and suggestions. The first author (J.S.) is financially supported by the US Office of Naval Research under Grant N00014-10-1-0453 and Grant N00014-12-1-0534.

Appendix A. Depth-induced wave breaking models

Here we provide a summary of the parameterizations of depth-induced breaking that have been assessed in the present study. It is not our purpose here to provide an extensive review; such reviews can be found in e.g. Rattanapitikon (2007) and Apotsos et al. (2008).

A.1. The Battjes–Janssen model

The Battjes–Janssen model assumes $H_{max} \approx d$ which results in a bulk dissipation:

$$\varepsilon_{BJ} = -\frac{1}{4}\alpha_{BJ}\bar{f}Q_b\rho g H_{max}^2 \tag{A1}$$

where α is a tunable coefficient of O(1), $\bar{f} = f_{m_{01}}$ and Q_b is the fraction of breakers:

$$\frac{1-Q_b}{lnQ_b} = -\left(\frac{H_{rms}}{H_{max}}\right)^2 \tag{A2}$$

The bulk dissipation is scaled with $\gamma_{BJ} = H_{\max}/d$; the simplest scalings are given by:

- Battjes and Janssen (1978): $\gamma_{BJ} = 0.80$
- Nelson (1985, 1987, 1994a,b, 1997):$\gamma_{BJ} = 0.55$
- *SWAN et al.: $\gamma_{BJ} = 0.73$

*Formulations used in this study are indicated here and below with an asterisk (*).

Nelson (1985, 1987, 1994a,b, 1997) has long advocated $\gamma_{BJ} = 0.55$ for waves over horizontal bathymetries in (very) shallow water. Such low values ($0.45 < \gamma_{BJ} < 0.65$) for irregular waves are supported by a variety of field and laboratory observations (e.g. Keating and Webber, 1977; Tucker et al., 1983; Riedel and Byrne, 1986; Hardy et al., 1990; Sulaiman et al., 1994; Hardy and Young, 1996; Moritz, 2001). Katsardi (2007) shows with numerical experiments that for irregular waves in finite depth water over a horizontal profile, $\gamma_{BJ} = 0.54$. Horikawa and Kuo (1966, their Figs. 5 and 3 as analyzed by Dally et al., 1985) find $\gamma_{BJ} \approx 0.25$.

Massel (1998) gives theoretical support for $\gamma_{BJ} \leqslant 0.55$. In very shallow water, a wave in an irregular wave field may behave as a solitary wave. The theoretical limit for the *crest* height of a solitary wave over a horizontal profile has been variously estimated from $\eta_{crest} = 1.78d$ (McCowan, 1894) to $\eta_{crest} = 1.86d$ (Longuet-Higgins, 1974) where d is the far field depth (i.e., undisturbed by the waves). If we take the average depth $\bar{d}$ to lie half way between the trough elevation $\eta_{trough} = d$ and the crest elevation $\eta_{crest} = \beta d$ (Seyama and Kimura, 1988; Kamphuis, 1991), then $H/\bar{d} = [\beta - 1]/[1 + (\beta - 1)/2]$. This yields $1.78 \leqslant \beta \leqslant 1.86$, so $0.56 \leqslant H/\bar{d} \leqslant 0.60$. A low value of $\gamma_{BJ} = 0.50$ was also found to be needed on a relatively steep beach (slope ~1:38) in the SWAN computations of Gorrell et al. (2011).

Several dependencies on bottom slope have been suggested based on a suggestion of Madsen (1976) for regular waves. His expression was modified by Ostendorf and Madsen (1979) to include wave-steepness induced breaking and subsequently modified by Rattanapitikon and Shibayama (2000). Although these scalings have been applied to irregular waves e.g. Black and Rosenberg (1992), Gonzalez-Roderiguez (2006) and Zheng et al. (2008), due to their inclusion of steepness-induced breaking (i.e. white capping), they are not applicable to our study.

- *Madsen (1976): $\gamma_{BJ} = 0.72(1 + 6.4\tan\beta)$
- Ostendorf and Madsen (1979, reduced):
  $\gamma_{BJ} = \begin{cases} 0.8 + 5\tan\beta & \tan\beta < 0.1 \\ 1.3 & \tan\beta \geqslant 0.1 \end{cases}$
- Rattanapitikon and Shibayama (2000):
  $\gamma_{BJ} = 0.91 + 5.01\tan\beta - 11.21\tan^2\beta$
- *Tajima and Madsen (2002): $\gamma_{BJ} = 0.3 + 4\tan\beta$

All these formulations suggest a positive dependency with a lower limit over a horizontal profile between $0.3 \leqslant \gamma_{BJ} \leqslant 0.91$. It may be noted, without further comment, that Raubenheimer et al. (1996) find for the ratio of *significant* wave height over depth, on the basis of field observations, a similar positive trend with bottom slope $\gamma_s = H_{m0}/d = 0.2 + 5.98\tan\beta$.

Although we did not find scalings of the form $\gamma_{BJ}(k_pd)$ in the literature, the laboratory observations of irregular waves over a 1:35 slope of Ting (2001, his Fig. 6) demonstrated an almost linear increase of γ_{BJ} (from 0.43 to 1.21) with k_pd (from 0.253 to 0.735; see Fig. A1). Our least-squares best fit gives a range of $0.56 \leqslant \gamma_{BJ} \leqslant 1.29$.

- *Ting (2001): $\gamma_{BJ} = 0.17 + 1.53k_pd$

A.2. The Thornton–Guza model

The Thornton–Guza model shifts the Rayleigh distribution for the breaking waves to higher wave heights with a weighting function $W_{TG}(H)$:

$$W_{TG}(H) = M_{TG}\left\{1 - \exp\left[-\left(\frac{H}{\gamma_{TG}d}\right)^2\right]\right\} \leqslant 1 \tag{A3}$$

where $M_{TG} = (H_{rms}/\gamma_{TG}d)^2$. The bulk dissipation is then given as:

$$\varepsilon_{TG} = -\frac{3\sqrt{\pi}}{16}\alpha_{TG}\bar{f}\rho g\frac{H_{rms}^3}{d}M_{TG}\left[1 - \frac{1}{\left(1 + (H_{rms}/(\gamma_{TG}d))^2\right)^{5/2}}\right] \tag{A4}$$

Most scalings for γ_{TG} depend on β:

- Thornton and Guza (1983): $\gamma_{TG} = 0.42$
- *Sallenger and Holman (1985): $\gamma_{TG} = 0.3 + 3.2\tan\beta$
- *Sallenger and Howd (1989): $\gamma_{TG} = 0.24 + 2.7\tan\beta$
- *Lippmann et al. (1996): $\gamma_{TG} = 0.23 + 1.42\tan\beta$

Thornton and Guza (1983) find (on average) that $\alpha_{TG} \approx 0.5$ for laboratory conditions and $\alpha_{TG} \approx 3.4$ for field conditions. Whitford (1988) finds $\alpha_{TG} \approx 0.98$ (average from his Figs. 50–52) from calibrating the expression of Sallenger and Holman (1985) to his γ_{TG} field observations using his modified conditional probability of breaking. However, Sallenger and Howd (1989) find ~20% lower values in their additional observations. Rattanapitikon (2007, his Table 3) finds in his calibration study very different values $\gamma_{TG} = 0.168$ and $\alpha_{TG} = 0.10$. With calibrated γ_{TG} values, Lippmann et al. (1996) predict the H_{rms} through the surf zone with practically the same error as the original Thornton and Guza (1983) model with $\alpha_{TG} = 1.0$ and calibrated γ_{TG} values. Lippmann et al. (1996) provides an approximation of $\gamma_{TG} = \tan^{0.4}\beta$ with $\alpha_{TG} = 1.0$. We approximate this with a least-square linear fit (see Fig. A1) to avoid $\gamma_{TG} = 0$ over horizontal bathymetries. Using linear wave theory, we infer that these observations (Lippmann et al., 1996, their Fig. 2 and Table 1) were made for the range $0.09 < k_pd < 0.42$.

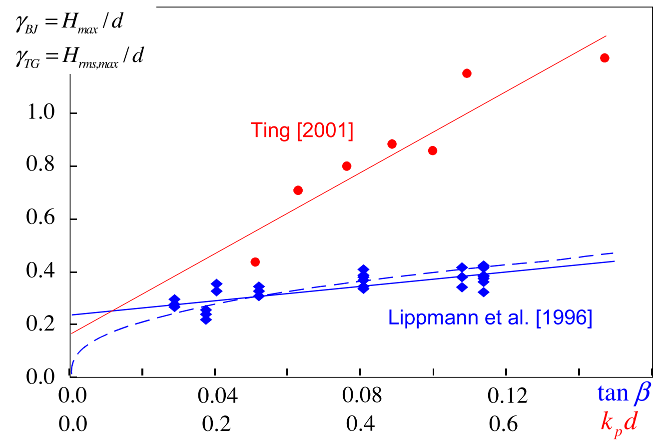

Fig. A1. The approximation by the present authors of the γ_{BJ} estimates of Ting (2001) as a function k_pd (for $\tan\beta = 1/35$; solid red line) and the γ_{TG} estimates of Lippmann et al. (1996) as a function of $\tan\beta$ (for $0.09 < k_pd < 0.42$; solid blue line). The power relationship with local bottom slope approximation of Lippmann et al. (1996) for γ_{TG} is also presented for reference (dashed blue line). (For interpretation of the references to color in this figure legend, the reader is referred to the web version of this article.)

A.3. The Baldock et al. model

Baldock et al. (1998) provide an explicit expression for Q_b:

$$Q_b = \exp[-(H_b/H_{rms})^2] \tag{A5}$$

and an expression for the bulk energy dissipation, originally formulated as:

$$\varepsilon_B^* = -\frac{\alpha_B}{4}\bar{f}\rho gH_{rms}^2(1 + R^2)\exp[-R^2] \tag{A6}$$

but later corrected by Janssen (2006), Janssen and Battjes (2007) and Alsina and Baldock (2007) to:

$$\varepsilon_B = -\frac{3\sqrt{\pi}}{16}\alpha_B\bar{f}\rho g \times \frac{H_{rms}^3}{d}\left[1 + \frac{4}{3\sqrt{\pi}}\left(R^3 + \frac{3}{2}R\right)\exp[-R^2] - erf(R)\right] \tag{A7}$$

in which $R = H_b/H_{rms}$. In the original work, the expression by Nairn (1990) was used, however due to its dependency on deep water wave steepness, it is not suitable for our purposes. The only scaling we found applicable was:

- *Ruessink et al. (2003): $\gamma_B = 0.29 + 0.76k_pd$

This scaling is based on a large number of field cases and inverse modeling. These γ_B values ($0.48 \leqslant \gamma_B \leqslant 0.86$ over the experimental range $0.25 \leqslant k_pd \leqslant 0.75$) are considerably lower than the γ_{BJ} values of Ting (2001) which were taken over virtually the same k_pd range. This is remarkable as nominally both γ_{BJ} and γ_B are the upper limit of the non-breaking (irregular) waves, but then, one data set was calibrated with field observations and the other was directly observed in a laboratory flume.

Raubenheimer et al. (1996) found a better fit with their observations by adding a k_pd dependency: $\gamma_s = 0.19 + 1.05\tan\beta/(k_pd)$. Sénéchal et al. (2001) also found a similar inverse trend but with considerably higher γ_s values. This is opposite to the trend found in Ting (2001) and Ruessink et al. (2003), however these observations relate to individual wave heights and not to the significant wave height.

A.4. The Dally et al./Rattanapitikon model

Rattanapitikon et al. (2003b, their Eq. (28)) gives an expression for bulk dissipation which does not depend on deep water parameters:

$$\varepsilon_D = -\frac{K_1 c_g \rho g}{8d}[H^2_{rms} - H^2_{rms,st}] \tag{A8}$$

in which c_g is the group velocity of the peak frequency (W. Rattanapitikon, pers. comm., 2012). We use Rattanapitikon (2007, his M37 model) to scale the dissipation with $\gamma_D = H_{rms,st}/d = 0.266$ as this is shown in that study to be the best performing model suitable for 2D spectral wave models.

Appendix B. Spectral distribution for the bulk dissipation

In all parameterizations, apart from the implementation of Filipot and Ardhuin (2012), the source term for depth-induced breaking is taken as proportional to the spectral density:

$$S(\sigma,\theta) = \varepsilon_b E(\sigma,\theta)/E \tag{B1}$$

Support for this spectral distribution is given by the observations of Beji and Battjes (1993) who observed that the *shape* of the wave spectrum seems to be unaffected by wave breaking. This seems to be inconsistent with the change of the spectrum during breaking. Initially, at the outer edge of the surf zone, higher harmonics of the spectral peak are generated, evident as secondary peaks, but deeper in the surf zone, these peaks typically disappear and the tail of the spectrum becomes featureless (Smith, 2004; Kaihatu et al., 2007 and Kaihatu et al., 2008). Such evolution seems to be almost entirely due to triad wave–wave interactions (Herbers et al., 2000) and not the breaking process. Even if the spectral distribution of Eq. (B1) is only approximately correct, triad wave–wave interactions will force the universal shape of the tail (Chen et al., 1997; Eldeberky, 2011). There are strong indications that the dissipation is actually proportional to σ^2 (Mase and Kirby, 1992; Kaihatu and Kirby, 1995; Kirby and Kaihatu, 1996; Chen et al. 1997). However, we consider these issues to be outside the scope of this paper as we are mostly concerned with the bulk dissipation (the prediction of the significant wave height) which is virtually independent of the spectral shape.

To verify the insensitivity between the proposed parameterization in this paper and the triad source term used, we also calibrated and verified our parameterization with the triad source term switched off (not shown). Over the verification data sets, the differences in model performance for the prediction of H_{m0} was negligible.

Appendix C. Supplementary data

Supplementary data associated with this article can be found, in the online version, at http://dx.doi.org/10.1016/j.ocemod.2014.12.011.

References

Alsina, J.M., Baldock, T.E., 2007. Improved representation of breaking wave energy dissipation in parametric wave transformation models. Coastal Eng. 54, 765–769.

Apotsos, A., Raubenheimer, B., Elgar, S., Guza, R.T., 2008. Testing and calibrating parametric wave transformation models on natural beaches. Coastal Eng. 55, 224–235.

Ardhuin, F., Herbers, T.H.C., O'Reilly, W.C., 2001. A hybrid Eulerian–Lagrangian model for spectral wave evolution with application to bottom friction on the continental shelf. J. Phys. Oceanogr. 31, 1498–1516.

Babanin, A.V., Hsu, T.-W., Roland, A., Ou, S.-H., Doong, D.-J., Kao, C.C., 2011. Spectral wave modelling of typhoon Krosa. Nat. Hazards Earth Syst. Sci. 11, 501–511.

Baldock, T.E., Holmes, P., Bunker, S., van Weert, P., 1998. Cross-shore hydrodynamics within an unsaturated surf zone. Coastal Eng. 34, 173–196.

Battjes, J.A., Janssen, J.P.F.M., 1978. Energy loss and set-up due to breaking of random waves. In: Proc. 16th Int. Conf. Coastal Eng.. ASCE, Hamburg, pp. 569–587.

Battjes, J.A., Janssen, T.T., 2008. Random wave breaking models – history and discussion. In: Proc. 31st Int. Conf. Coastal Eng.. World Scientific, pp. 25–37.

Battjes, J.A., Stive, M.J.F., 1985. Calibration and verification of a dissipation model for random breaking waves. J. Geophys. Res. 90 (C5), 9159–9167.

Beji, S., Battjes, J.A., 1993. Experimental investigation of wave propagation over a bar. Coastal Eng. 19, 151–162.

Benoit, M., Marcos, F., Becq, F., 1996. Development of a third generation shallow-water wave model with unstructured spatial meshing. In: Proc. 25th Int. Conf. Coastal Eng.. ASCE, Orlando, pp. 465–478.

Black, K.P., Rosenberg, M.A., 1992. Semi-empirical treatment of wave transformation outside and inside the breaker line. Coastal Eng. 16, 313–345.

Boers, M., 2005. Surf zone turbulence (Ph.D. thesis). Delft University of Technology, 171 pp., also as Commun. Hydr. Geotech. Eng., 05–3, 171p.

Booij, N., Ris, R.C., Holthuijsen, L.H., 1999. A third-generation wave model for coastal regions. Part I: Model description and validation. J. Geophys. Res. 104 (C4), 7649–7666.

Bottema, M., Beyer, D., 2002. Evaluation of the SWAN wave model for the Dutch IJsselmeer area. In: Edge, B.L., Michael Hemsley, J. (Eds.), Ocean Wave Measurement and Analysis. Am. Soc. of Civil Eng., Reston, VA, pp. 560–569.

Bottema, M., van Vledder, G.Ph., 2009. A ten-year data set for fetch- and depth-limited wave growth. Coastal Eng. 56, 703–725.

Bottema, M., de Waal, J.P., Regeling, H.J., 2002. Some applications of the Lake IJssel/Lake Sloten wave data set. In: 28th Int. Conf. Coastal Eng.. World Scientific, pp. 413–425.

Bretherton, F.P., Garrett, C.J.R., 1968. Wavetrains in inhomogeneous moving media. Proc. R. Soc. London A 302 (1471), 529–554. http://dx.doi.org/10.1098/rspa.1968.0034.

Camenen, B., Larson, M., 2007. Predictive formulas for breaking depth index and breaker type. J. Coastal Res. 23 (4), 1028–1041.

Chen, Y., Guza, R.T., Elgar, S., 1997. Modeling spectra of breaking surface waves in shallow water. J. Geophys. Res. 102 (C11), 25035–25046.

Coates, T.T., Jones, R.J., Bona, P., 1998. Wave flume studies on responses to wind/swell seas and steep approach slopes. Res. Rep. TR 24, HR Wallingford.

Dally, W.R., 1992. Random breaking waves: field verification of a wave-by-wave algorithm for engineering applications. Coastal Eng. 16, 369–397.

Dally, W.R., Dean, R.G., Dalrymple, R.A., 1985. Wave height variation across beaches of arbitrary profile. J. Geophys. Res. 90 (C6), 11917–11927.

De Waal, J.P., 2002. Wave growth limit in shallow water. In: Edge, B.L., Michael Hemsley, J. (Eds.), Ocean Wave Measurement and Analysis. ASCE, Reston, VA, pp. 580–589.

Demirbilek, Z., Nwogu, O.G., Ward, D.L., 2007. Laboratory study of wind effect on runup over fringing reefs, Report 1: data report, US Army Corps of Engineers, U.S. Army Engineer Research and Development Center, Coastal and Hydraulics Laboratory, Rep. ERDC/CHL TR-07-4, 82p.

Dietrich, J.C., Tanaka, S., Westerink, J.J., Dawson, C.N., Luettich Jr., R.A., Zijlema, M., Holthuijsen, L.H., Smith, J.M., Westerink, L.G., Westerink, H.J., 2013. Performance of the unstructured-mesh SWAN+ADCIRC model in computing hurricane waves and surge. J. Sci. Comput. http://dx.doi.org/10.1007/s10915-011-9555-6.

Dingemans, M.W., 1987. Verification of numerical wave propagation models with laboratory measurements, HISWA verification in the directional wave basin, Delft Hydraulics, Rep. No. H228.

Dingemans, M.W., Stive, M.J.F., Bosma, J., de Vriend, H.J., Vogel, J.A., 1986. Directional nearshore wave propagation and induced currents. In: Proc. 20th Int. Conf. Coastal Eng.. ASCE, Taipei, pp. 1092–1106.

Eldeberky, Y., 1996. Nonlinear transformation of wave spectra in the nearshore zone (Ph.D. thesis). Delft University of Technology, Department of Civil Engineering, The Netherlands, 203p also as Commun. Hydr. Geotech. Eng., 96-4, 203p.

Eldeberky, Y., 2011. Modeling spectra of breaking waves propagating over a beach. Ain Shams Eng. J. 2, 71–77.

Fenton, J.D., 1990. Nonlinear wave theories. In: LeMéhauté, B., Hanes, D.M. (Eds.), The Sea, Ocean Engineering Science, vol. 9. Wiley, New York, 18p.

Filipot, J.-F., Ardhuin, F., 2012. A unified parameterization for wave breaking: from the deep ocean to the surf zone. J. Geophys. Res. 117, C00J08. http://dx.doi.org/10.1029/2011JC007784.

Goda, Y., 2004. A 2-D random wave transformation model with gradational breaking index. Coastal Eng. J. 46 (1), 1–38.

Goda, Y., 2009. A performance test of nearshore wave height prediction with CLASH datasets. Coastal Eng. 56, 220–229.

Goda, Y., 2010. Reanalysis of regular and random breaking wave statistics. Coastal Eng. J. 52 (1), 71–106.

Gonzalez-Rodriguez, D., 2006. Modeling of Nearshore Hydrodynamics for Sediment Transport Calculations. (Ph.D. thesis). Massachusetts Institute of Technology, 133p.

Gorrell, L., Raubenheimer, B., Elgar, S., Guza, R.T., 2011. SWAN predictions of waves observed in shallow water onshore of complex bathymetry. Coastal Eng. 58, 510–516.

Graber, H.C., Madsen, O.S., 1988. A finite-depth wind-wave model. Part I: Model description. J. Phys. Oceanogr. 18, 1465–1483.

Green, M.O., Coco, G., 2014. Review of wave-driven sediment resuspension and transport in estuaries. Rev. Geophys. 52, 77–117. http://dx.doi.org/10.1002/2013RG000437.

Groeneweg, J., van Vledder, G., Hurdle, D., Doorn, N., Kuiper, C., 2003. Reliability of SWAN at the Petten sea defense. Rep. No. H4197/A1044, WL|Delft Hydraulics & Alkyon.

Groeneweg, J., van der Westhuysen, A., van Vledder, G., Jacobse, S., Lansen, J., van Dongeren, A., 2008. Wave Modelling in a tidal inlet: performance of SWAN in the Wadden Sea. In: 31st Int. Conf. Coastal Eng.. World Scientific, pp. 411–423.

Hanson, J.L., Phillips, O.M., 2001. Automated analysis of ocean surface directional wave spectra. J. Atmos. Ocean Tech. 18, 277–293.

Hardy, T.A., Young, I.R., 1996. Field study of wave attenuation on an offshore coral reef. J. Geophys. Res. 101 (C6), 14311–14326.

Hardy, T.A., Young, I.R., Nelson, R.C., Gourlay, M.R., 1990. Wave attenuation on an offshore reef. In: 22nd Int. Conf. Coastal Eng.. ASCE, Delft, pp. 330–344.

Hasselmann, K., 1974. On the spectral dissipation of ocean waves due to white capping. Bound.-Layer Meteorol. 6 (1–2), 107–127.

Hasselmann, K., Barnett, T.P., Bouws, E., Carlson, H., Cartwright, D.E., Enke, K., Ewing, J.A., Gienapp, H., Hasselmann, D.E., Kruseman, P., Meerburg, A., Müller, P., Olbers, D.J., Richter, K., Sell, W., Walden, H., 1973. Measurements of wind-wave growth and swell decay during the Joint North Sea Wave Project (JONSWAP). Dtsch. Hydrogr. Z. Suppl. A8 (12), 95.

Hasselmann, S., Hasselmann, K., Allender, J.H., Barnett, T.P., 1985. Computations and parameterizations of the nonlinear energy transfer in a gravity wave spectrum. Part II: Parameterizations of the nonlinear transfer for application in wave models. J. Phys. Oceanogr. 15 (11), 1378–1391.

Hawkes, P.J., Coates, T.T., Jones, R.J., 1998. Impact of bi-modal seas on beaches and control structures. Res. Rep. SR 507, HR Wallingford.

Herbers, T.H.C., Russnogle, N.R., Elgar, S., 2000. Spectral energy balance of breaking waves within the surf zone. J. Phys. Oceanogr. 30, 2723–2737.

Holthuijsen, L.H., 2007. Waves in Oceanic and Coastal Waters. Cambridge University Press, Cambridge, 404p.

Holthuijsen, L.H., Booij, N., 2006. Experimental wave breaking in SWAN. In: 30th Int. Conf. Coastal Eng.. World Scientific, pp. 392–402.

Horikawa, K., Kuo, C.-T., 1966. A study on wave transformation inside surf zone. In: Tenth Int. Conf. Coastal Eng.. ASCE, Tokyo, pp. 217–233.

Janssen, T.T., 2006. Nonlinear Surface Waves Over Topography (Ph.D. thesis). Delft University of Technology (Library Repository), 208p.

Janssen, T.T., Battjes, J.A., 2007. A note on wave energy dissipation over steep beaches. Coastal Eng. 54, 711–716.

Janssen, P.A.E.M., Komen, G.J., de Voogt, W.J.P., 1984. An operational coupled hybrid wave prediction model. J. Geophys. Res. 89 (C3), 3635–3654.

Jensen, M.S., 2002. Breaking of Waves Over a Steep Bottom Slope (Ph.D. thesis). Hydraulics & Coastal Engineering Laboratory, Department of Civil Engineering, Aalborg University, Denmark, ISSN 0909-4296, Series paper No. 22, 162p.

Kaihatu, J.M., Kirby, J.T., 1995. Nonlinear transformation of waves in finite water depth. Phys. Fluids 7 (8), 1903–1914.

Kaihatu, J.M., Veeramony, J., Edwards, K.L., Kirby, J.T., 2007. Asymptotic behavior of frequency and wave number spectra of near shore shoaling and breaking waves. J. Geophys. Res. 112, C06016. http://dx.doi.org/10.1029/2006JC003817.

Kaihatu, J.M., Veeramony, J., Edwards, K.L., 2008. Spatial evolution of the frequency distribution of dissipation and implications on frequency domain modeling. In: Proc. 31st Int. Conf. Coastal Eng., Hamburg, Germany. ASCE, New York, pp. 293–301.

Kamphuis, J.W., 1991. Incipient wave breaking. Coastal Eng. 15, 185–203.

Katsardi, V., 2007. Surface Water Waves in Intermediate and Shallow Water Depths (Ph.D. thesis). Imperial College, London, 270p.

Katsardi, V., de Lutio, L., Swan, C., 2013. An experimental study of large waves in intermediate and shallow water depths. Part I: Wave height and crest height statistics. Coastal Eng. 73, 43–57.

Keating, T., Webber, N.B., 1977. The generation of periodic waves in a laboratory channel: a comparison between theory and experiment. Proc. Inst. Civil Eng., Part 2 63, 819–832.

Kirby, J.T., Kaihatu, J.M., 1996. Structure of frequency domain models for random wave breaking. In: Proc. 25th Int. Conf. Coastal Eng., Orlando, FL. ASCE, New York, pp. 1144–1155.

Komen, G.J., Hasselmann, S., Hasselmann, K., 1984. On the existence of a fully developed wind–sea spectrum. J. Phys. Oceanogr. 14 (8), 1271–1285.

Komen, G.J., Cavaleri, L., Donelan, M., Hasselmann, K., Hasselmann, S., Janssen, P.A.E.M., 1994. Dynamics and Modelling of Ocean Waves. Cambridge University Press, Cambridge, 532p.

Kuik, A.J., van Vledder, G.Ph., Holthuijsen, L.H., 1988. A method for the routine analysis of pitch-and-roll buoy wave data. J. Phys. Oceanogr. 18 (7), 1020–1034.

Lamb, H., 1932. Hydrodynamics, sixth ed. Dover Publications, New York, 738p.

Latheef, M., Swan, C., 2013. A laboratory study of wave crest statistics and the role of directional spreading. Proc. R. Soc. A, 469, No. 2152.

LeMéhauté, B., 1962. On non-saturated breakers and the wave run-up. In: Proc. Eighth Conf. Coastal Engineering, Mexico City. ASCE, New York, pp. 77–92.

Lentz, S.J., Howd, M.F.P., Fredericks, J., Hathaway, K., 2008. Observations and a model of undertow over the inner continental shelf. J. Phys. Oceanogr. 38, 2341–2357.

Lippmann, T.C., Brookins, A.H., Thornton, E.B., 1996. Wave energy transformation on natural profiles. Coastal Eng. 27, 1–20.

Longuet-Higgins, M.S., 1952. On the statistical distributions of the heights of sea waves. J. Mar. Res. 11 (3), 245–265.

Longuet-Higgins, M.S., 1974. On the mass, momentum, energy and circulation of a solitary wave. Proc. R. Soc. A 337, 1–13.

Lowe, R.J., Falter, J.L., Monismith, S.G., Atkinson, M.J., 2009a. A numerical study of circulation in a coastal reef-lagoon system. J. Geophys. Res. 114, C06022. http://dx.doi.org/10.1029/2008JC005081.

Lowe, R.J., Falter, J.L., Monismith, S.G., Atkinson, M.J., 2009b. Wave-driven circulation of a coastal reef-lagoon system. J. Phys. Oceanogr. 39, 873–893. http://dx.doi.org/10.1175/2008JPO3958.1.

Madsen, O.S., 1976. Wave climate of the continental margin: elements of its mathematical description. In: Stanley, D.J., Swift, D.J.P. (Eds.), Marine Sediment Transport in Environmental Management. Wiley, New York, pp. 65–87, cited by Rattanapitikon and Shibayama (2000).

Mase, H., Kirby, J.T., 1992. Hybrid frequency-domain KdV equation for random wave transformation. In: Proc. 23rd Int. Conf. Coastal Eng., Venice. ASCE, New York, pp. 474–487.

Massel, S.R., 1998. The limiting wave height in wind-induced wave trains. Ocean Eng. 25 (9), 735–752.

McCowan, J., 1894. On the highest wave of permanent type. Philos. Mag. Ser. 5 (32), 351–358, Cited by Longuet-Higgins (1974).

Miche, R., 1944. Mouvements ondulatoires des mers en profondeur constante ou décroissante. Ann. Ponts Chaussées, 369–406.

Monbaliu, J., Padilla-Hernández, R., Hargreaves, J.C., Carretero Albiach, J.C., Luo, W., Sclavo, M., Günther, H., 2000. The spectral wave model, WAM, adapted for applications with high spatial rsolution. Coastal Eng. 41, 41–62.

Moritz, H.R., 2001. Observing large waves using bottom-mounted pressure and current meters. In: Edge, B.L., Michael Hemsley, J. (Eds.), Ocean Wave Measurement and Analysis. ASCE, Reston, VA, pp. 44–53.

Mulligan, R.P., Hay, A.E., Bowen, A.J., 2010. A wave-driven jet over a rocky shoal. J. Geophys. Res. 115, C10038. http://dx.doi.org/10.1029/2009JC006027.

Nairn, R.B., 1990. Prediction of Cross-Shore Sediment Transport and Beach Profile Evolution (Ph.D. thesis) Imperial College, London, 391p.

Nelson, R.C., 1985. Wave heights in depth limited conditions. Civil Eng. Trans. Inst. Eng. Aust. CE27, 210–215.

Nelson, R.C., 1987. Design wave heights on very mild slopes – an experimental study. Civil Eng. Trans. Inst. Eng. Aust. 29, 157–161.

Nelson, R.C., 1994a. Depth limited design wave heights in very flat regions. Coastal Eng. 23, 43–59.

Nelson, R.C., 1994b. Height limit anomalies in laboratory waves. In: Int. Symp.: Waves – Physical and Numerical Modelling. Univ. British Columbia, Vancouver, Canada, pp. 580–589.

Nelson, R.C., 1997. Height limits in top down and bottom up wave environments. Coastal Eng. 32, 247–254.

Onarato, M., Cavaleri, L., Fouques, S., Gramstad, O., Janssen, P.A.E.M., Monbaliu, J., Osborne, A.R., Pakozdi, C., Serio, M., Stansberg, C.T., Toffoli, A., Trulsen, K., 2009. Statistical properties of mechanically generated surface gravity waves: a laboratory experiment in a three-dimensional wave basin. J. Fluid Mech. 627, 235–257.

Ostendorf, D.W., Madsen, O.S., 1979. An analysis of long-shore current and associated sediment transport in the surf zone. Report No. 241, Department of Civil Engineering, MIT, 169p (cited by Rattanapitikon and Shibayama (2000) and Camenen and Larson (2007)).

Péquignet, A.-C., Becker, J.M., Merrifield, M.A., Boc, S.J., 2011. The dissipation of wind wave energy across a fringing reef at Ipan, Guam. Coral Reefs 30, 71–82.

Phillips, O.M., 1977. The Dynamics of the Upper Ocean. Cambridge University Press, Cambridge, 336p.

Rattanapitikon, W., 2007. Calibration and modification of energy dissipation models for irregular wave breaking. Ocean Eng. 34, 1592–1601.

Rattanapitikon, W., Shibayama, T., 1998a. Energy dissipation model for irregular breaking waves. In: 26th Int. Conf. Coastal Eng.. ASCE, Copenhagen, pp. 112–125.

Rattanapitikon, W., Shibayama, T., 1998b. Energy dissipation model for regular and irregular breaking waves. Coastal Eng. J. 40 (4), 327–346.

Rattanapitikon, W., Shibayama, T., 2000. Verification and modification of breaker height formulas. Coastal Eng. J. 42 (4), 389–406.

Rattanapitikon, W., Vivattanasirisak, T., Shibayama, T., 2003a. A proposal of new breaker height formula. Coastal Eng. J. 45 (1), 29–48.

Rattanapitikon, W., Karunchintadit, R., Shibayama, T., 2003b. Irregular wave height transformation using representative wave approach. Coastal Eng. J. 45 (3), 489–510.

Raubenheimer, B., Guza, R.T., Elgar, S., 1996. Wave transformation across the inner surf zone. J. Geophys. Res. 101 (C10), 25589–25597.

Riedel, H.P., Byrne, A.P., 1986. Random breaking waves – horizontal seabed. In: 20th Int. Conf. Coastal Eng.. ASCE, Taipei, pp. 903–908.

Ris, R.C., Booij, N., Holthuijsen, L.H., 1999. A third-generation wave model for coastal regios. Part II. Verification. J. Geophys. Res. 104 (C4), 7667–7681.

Roelvink, J.A., 1993. Dissipation in random wave groups incident on a beach. Coastal Eng. 19, 127–150.

Rogers, W.E., Hwang, P.A., Wang, D., 2003. Investigation of wave growth and decay in the SWAN model: three regional-scale applications. J. Phys. Oceanogr. 33, 366–389.

Roland, A., 2009. Development of the WWM (Wind Wave Model) II: Spectral Wave Modelling on Unstructured Meshes (Ph.D. thesis). Mitteilungen, Heft 146, Inst. of Hydraul. And Water Resour. Eng., Techn. Univer. Darmstadt, 212p.

Roland, A., Zanke, U., Hsu, T.-W., Ou, S.-H., Liau, J.-M., 2006. Spectral wave modelling on unstructured grids with WWM (Wind Wave Model) I: the deep water case.

In: Third Chinese–German Joint Symposium on Coastal and Ocean Engineering, National Cheng Kung University, Tainan.
Ruessink, B.G., Walstra, D.J.R., Southgate, H.N., 2003. Calibration and verification of a parametric wave model on barred beaches. Coastal Eng. 48, 139–149.
Sallenger, A.H., Holman, R.A., 1985. Wave energy saturation on a natural beach of variable slope. J. Geophys. Res. 90 (C6), 11939–112944.
Sallenger, A.H., Howd, P.A., 1989. Nearshore bars and the break-point hypothesis. Coastal Eng. 12, 301–313.
Sénéchal, N., Dupuis, H., Bonneton, Ph., Howa, H., Pedreros, R., 2001. Observation of irregular wave transformation in the surf zone over a gently sloping sandy beach on the French Atlantic coastline. Oceanol. Acta 24 (6), 545–556.
Seyama, A., Kimura, A., 1988. The measured properties of irregular wave breaking and wave height change after breaking on the slope. In: 21st Int. Conf. Coastal Eng.. ASCE, Torremolinos, pp. 419–432.
Smith, J.M., 2004. Shallow-water spectral shapes. In: 29th Int. Conf. Coastal Eng.. World Scientific, pp. 206–217.
Snyder, R.L., Dobson, F.W., Elliott, J.A., Long, R.B., 1981. Array measurement of atmospheric pressure fluctuations above surface gravity waves. J. Fluid Mech. 102, 1–59.
Sørensen, O.R., Kofoed-Hansen, H., Rugbjerg, M., Sørensen, L.S., 2004. A third generation spectral wave model using an unstructured finite volume technique. In: 29th Int. Conf. Coastal Eng.. World Scientific, pp. 894–906.
Stoker, J.J., 1957. Water Waves. Interscience Publishers Inc., New York, 567p.
Sulaiman, D.M., Tsutsui, S., Yoshioka, H., Yamashita, T., Oshiro, S., Tsuchiya, Y., 1994. Prediction of the maximum wave on the coral flat. In: 24th Int. Conf. Coastal Eng.. ASCE, Kobe, pp. 609–623.
Svendsen, I.A., 1987. Analysis of surf zone turbulence. J. Geophys. Res. 92 (C5), 5115–5124.
Tajima, Y., Madsen, O.S., 2002. Shoaling, breaking and broken wave characteristics. In: 28th Int. Conf. Coastal Eng.. World Scientific, pp. 222–234.
Thornton, E.B., Guza, R.T., 1983. Transformation of wave height distribution. J. Geophys. Res. 88, 5925–5938.
Ting, F.C.K., 2001. Laboratory study of wave and turbulence velocities in a broad-banded irregular wave surf zone. Coastal Eng. 43, 183–208.
Tolman, H.L., 1990a. The influence of unsteady depths and currents of tides on wind-wave propagation in shelf seas. J. Phys. Oceanogr. 20, 1166–1174.
Tolman, H.L., 1990b. Wind Wave Propagation in Tidal Seas (Ph.D. thesis). Delft University of Technology (Library Repository), 195p.
Tolman, H.L., 2009. User manual and system documentation of WAVEWATCH III version 3.14. NOAA/NWS/NCEP/MMAB Technical Note 276, 194 pp.+ Appendices (0.83Mb pdf file).
Tolman, H.L., Chalikov, D., 1996. Source terms in a third-generation wind wave model. J. Phys. Oceanogr. 26, 2497–2518.
Tucker, M.J., Carr, A.P., Pitt, E.G., 1983. The effect of an offshore bank in attenuating waves. Coastal Eng. 7, 133–144.
Van der Meer, J.W., Hurdle, D.P., van Vledder, G.Ph., van Gent, M.R.A., Ris, R.C., 2000. Uni- and bi-modal spectra on steep foreshores – validation of the SWAN model, wave height statistics and wave overtopping, based on HR Wallingford data, Delft Hydraulics/Alkyon/INFRAM, Rep. i230/A509/H3510.
van der Westhuysen, A.J., 2009. Modelling of depth induced wave breaking over sloping and horizontal beds. In: 11th International Workshop on Wave Hindcasting and Forecasting, Halifax, WMO/IOC Joint Technical Commission for Oceanography and Marine Meteorology, 10p.
van der Westhuysen, A.J., 2010. Modeling of depth-induced wave breaking under finite depth wave growth conditions. J. Geophys. Res. 115, C01008. http://dx.doi.org/10.1029/2009JC005433.
van der Westhuysen, A.J., de Waal, J.P., 2008. Observed finite depth wave growth limit in the Wadden Sea, Deltares report H5107.35. 36 pp. +3 Appendices.
van der Westhuysen, A.J., Zijlema, M., Battjes, J.A., 2007. Nonlinear saturation-based whitecapping dissipation in SWAN for deep and shallow water. Coastal Eng. 54, 151–170.
van Vledder, G.Ph., Groeneweg, J., van der Westhuysen, A.J., 2008. Numerical and physical aspects of wave modeling in a tidal inlet. In: Proc. 31st Int. Conf. Coastal Eng.. World Scientific, pp. 424–436.
van Vledder, G.Ph., Ruessink, G., Rijnsdorp, D., 2013. Individual wave height distributions in the coastal zone: measurements and simulations and the effect of directional spreading. Coastal Dyn. 2013, 1799–1810.
Vincent, C.L., 1985. Depth-controlled wave height. J. Waterway Port Coastal Ocean Eng. 111 (33), 459–475.
Vink, A.S., 2001. Transformation of Wave Spectra Across the Surf Zone (M.Sc. thesis). Delft University of Technology (Library Repository), 72p.
WAMDI group, 1988. The WAM model – a third generation ocean wave prediction model. J. Phys. Oceanogr. 18 (12), 1775–1810.
Whitford, D.J., 1988. Wind and Wave Forcing of Longshore Currents across a Barred Beach (Ph.D. thesis). Naval Postgraduate School, Monterey, CA, 205p.
Young, I.R., Babanin, A.V., 2006. The form of the asymptotic depth-limited wind wave frequency spectrum. J. Geophys. Res. 111, C06031. http://dx.doi.org/10.1029/2005JC003398.
Zheng, J., Mase, H., Demirbilek, Z., Lin, L., 2008. Implementation and evaluation of alternative wave breaking formulas in a coastal spectral wave model. Ocean Eng. 35, 1090–1101.
Zijlema, M., 2010. Computation of wind-wave spectra in coastal waters with SWAN on unstructured grids. Coastal Eng. 57, 267–277.
Zijlema, M., van Vledder, G.Ph., Holthuijsen, L.H., 2012. Bottom friction and wind drag for spectral wave models. Coastal Eng. 65, 19–26.

Further reading

Boers, M., 1996. Simulations of a surf zone with a barred beach, report 1: Wave heights and wave breaking. Commun. Hydraul. Geotech. Eng. 69 (5), 116.
Bouws, E., Günther, H., Rosenthal, W., Vincent, C.L., 1985. Similarity of the wind wave spectrum in finite depth water. 1. Spectral form. J. Geophys. Res. 90 (C1), 975–986.
Demirbilek, Z., Nwogu, O.G., Ward, D.L., Sánchez, A., 2009. Wave transformation over reefs: evaluation of one-dimensional numerical models, US Army Corps of Engineers, US Army Engineer Research and Development Center, Coastal and Hydraulics Laboratory, Rep. ERDC/CHL TR-09-1, p. 207.
Hawkes, P.J., Jones, R.J., Durand, N., 1999. Supply and further analysis of TR 24 wave time series data. Rep. EX 4114, HR Wallingford.
Katsardi, V., Swan, C., 2011. An experimental study of shallow water wave statistics on mild bed slopes. In: 30th Int. Conf. Ocean, Offshore and Arctic Eng. OMAE2011, pp. 711–719.
Sheremet, A., Kaihatu, J.M., Su, S.-F., Smith, E.R., Smith, J.M., 2011. Modeling of nonlinear wave propagation over fringing reefs. Coastal Eng. 58, 1125–1137.
Su, S.-F., Sheremet, A., Smith, J.M., 2010. Parametric wave-breaking on steep reefs. In: 32nd Int. Conf. Coastal Eng.. Coastal Engineering Research Council.
Zijlema, M., 2012. Modelling wave transformation across a fringing reef using SWASH. In: Proc. 33rd Int. Conf. Coastal Eng.. Coastal Engineering Research Council.